Available online at www.sciencedirect.com
SCIENCE DIRECT
Icarus 172 (2004) 233–254
ICARUS
www.elsevier.com/locate/icarus

Mafic silicate mapping on Mars: effects of palagonitic material, multiple mafic silicates, and spectral resolution

Edward A. Cloutis [a,*], James F. Bell III [b]

[a] *Department of Geography, University of Winnipeg, 515 Portage Avenue, Winnipeg, MB, Canada R3B 2E9*
[b] *Department of Astronomy, Cornell University, 402 Space Sciences Building, Ithaca, NY 14853-6801, USA*

Received 14 November 2003; revised 20 April 2004

Available online 4 August 2004

Abstract

The visible to near-infrared spectral reflectance properties of intimate and areal pyroxene + palagonitic material mixtures as well as pure mafic silicates (low-calcium pyroxene, high-calcium pyroxene, pigeonite, olivine) and mixtures of these minerals were analyzed at high spectral resolution (5 nm) as well as with non-contiguous band passes equivalent to recent HST observations and the Pathfinder IMP in order to determine the quality and quantity of mineralogical information (end member compositions, abundances, and grain sizes) derivable in the presence of palagonitic material. In the case of pyroxene + palagonitic material mixtures, pyroxene is detectable at abundances as low as 10 wt%, and its composition can be constrained because (a) its diagnostic absorption feature (located near 1000 nm) persists even for high palagonitic material abundances, and (b) palagonitic material does not appreciably alter the wavelength position of this band (< 4 nm variation). For broad band data (such as Pathfinder IMP band passes), different mafic silicates can be discriminated and palagonitic material abundances constrained using a variety of reflectance ratios and three-point "absorption band depths." However, other properties of mafic silicate ± palagonitic material assemblages, such as mafic silicate major element compositions, grain sizes, and end member abundances, generally cannot be rigorously quantified. The use of multiple reflectance ratios can, however, be used to identify relative changes in these properties, as most changes in mafic silicate ± palagonitic material assemblage properties are characterized by a unique corresponding set of reflectance ratio variations. The observed spectral-assemblage property trends are consistent with those expected from the known spectral properties of the end members.

Keywords: Mars surface; Regoliths; Mineralogy; Spectrophotometry

1. Introduction

Pyroxenes are among the most widespread mafic silicates in the inner Solar System (e.g., McCord et al., 1970; McCord and Clark, 1979; Feierberg et al., 1980; Basaltic Volcanism Study Project, 1981; Dodd, 1981; Surkov et al., 1983; Huguenin, 1987; Cruikshank et al., 1991; Gaffey et al., 1993a, 1993b; McSween and Treiman, 1998) and one of the most well-characterized minerals spectrally (e.g., Adams, 1974; Hazen et al., 1978; Cloutis and Gaffey, 1991a). A knowledge of the compositional, structural, and textural properties of mafic silicate-bearing assemblages can provide important constraints on the formation conditions of targets in which these minerals reside (e.g., Wood and Banno, 1973; Morse, 1980; Lindsley, 1983; Lindsley and Andersen, 1983).

Pyroxenes are thought to be widespread on the surface of Mars on the basis of spectral studies (e.g., Singer, 1985; Pinet and Chevrel, 1990; Mustard et al., 1993b; Roush et al., 1993; Bell, 1996; Christensen et al., 1998, 2000; Bandfield et al., 2000; Morris et al., 2000) and known to be present from direct examination of martian meteorites (e.g., Wood and Ashwal, 1981; McSween and Treiman, 1998; Folco et al., 1999). Spectral deconvolution has been successfully applied to martian meteorite spectra to derive mafic

* Corresponding author. Fax: (204)-774-4134.
E-mail address: e.cloutis@uwinnipeg.ca (E.A. Cloutis).

0019-1035/$ – see front matter
doi:10.1016/j.icarus.2004.06.002

silicate compositional information (Sunshine et al., 1993; Bishop et al., 1998a).

For the martian meteorites, major element (Mg, Fe, Ca) composition, relative proportions of mafic silicates, and grain size/textural observations all allow the composition of parental magmas and formation conditions to be inferred, such as late stage differentiation, oxidation state, degree of partial melting, parental magma composition, cumulus formation, and degree of fractionation (Mason et al., 1975; Boctor et al., 1976; Floran et al., 1978; McSween et al., 1979; Smith and Hervig, 1979; Stolper and McSween, 1979; Stolper et al., 1979; Berkley et al., 1980; Wood and Ashwal, 1981; Smith et al., 1984; McSween and Jarosewich, 1983; McSween, 1985; Lundberg et al., 1990; Treiman, 1990; Murchie et al., 1993; Mikouchi et al., 1998). Conditions of formation as well as subsequent alteration/weathering can also be augmented with information from analysis of additional mineral phases that may be present. A knowledge of the mineralogy of martian extrusive lava flows and (exposed) intrusive igneous bodies (e.g., Mustard et al., 1997) can augment geomorphological (e.g., Mouginis-Mark, 1981; Cattermole, 1990; Greeley and Crown, 1990; Lopes and Kilburn, 1990; Gregg and Williams, 1996) and modeling studies (e.g., Solomon and Head, 1982; Finnerty et al., 1988) of these targets to help place constraints on mantle evolution, heat loss, viscosities, effusion conditions, rheology, and density. A more detailed knowledge of the mineralogy comprising these features would help to further constrain petrogenetic conditions derivable from geomorphology alone.

On Earth, economic deposits of metals such as chromium, platinum and platinum group metals, titanium, iron, and copper-nickel-iron are frequently associated with mafic silicate minerals (e.g., Evans, 1980; Eckstrand, 1984). Consequently an ability to detect mafic silicate occurrences and derive some compositional information could assist in the detection and mapping of similar deposits on Mars if they exist.

One of the major uncertainties inherent in constraining the composition and abundance of mafic silicates on Mars from analysis of reflectance spectroscopic data are the spectrum-altering effects of other phases which may be present (e.g., Cloutis and Gaffey, 1991b). A related problem is determining the minimum spectral resolution and wavelength coverage necessary for quantitative analysis of mafic silicate compositions from reflectance spectra. In the case of Mars, the major phase which may affect mafic silicate reflectance spectra is poorly crystalline ferric iron-bearing material (e.g., Bell et al., 1993; Morris et al., 1993, 1997; Murchie et al., 1993; Morris and Golden, 1998) which is spectrally similar to terrestrial palagonitic material, a common weathering product of basaltic tuffs (Moore, 1966; Hay and Iijima, 1968). A material spectrally similar to terrestrial palagonitic material has been found to be present across much of the martian surface and commonly blankets (partially or fully) outcrops of basaltic/andesitic materials (Johnson et al., 1999; McSween and Murchie, 1999; McSween et al., 1999; Bell et al., 2000).

Few visible to near-infrared (VIS-NIR) spectral reflectance studies of Mars have combined high spectral and spatial resolution on a planetary scale. Planetary-scale near-infrared observations at high spatial resolution generally have been conducted at low spectral resolution (e.g., Bell et al., 1997) or over only limited regions of the surface (Murchie et al., 1993; Mustard et al., 1993a). Similarly, landers such as Viking and Pathfinder have acquired high spatial resolution data around their landing sites but at only a few discrete wavelengths (Adams et al., 1986; McSween et al., 1999; Bell et al., 2000). For future lander/rover or orbiter regional- or global-scale multispectral geological mapping studies, it would be useful to determine what types of compositional information can be derived from quantitative analysis of existing or planned low spectral resolution observational data sets.

This study was designed to: (1) study the spectrum-altering effects of palagonitic material on pyroxene reflectance spectra, particularly in the 300–1000 nm region, in order to determine whether compositional information can still be derived in the presence of palagonitic material; (2) determine whether different mafic silicates can be discriminated using lower spectral resolution data such as that available from recent observations of Mars using the Hubble Space Telescope (HST) Wide Field/Planetary Camera 2 (WFPC2) (Bell et al., 1997), the Imager for Mars Pathfinder (IMP) camera (Smith et al., 1997), and the upcoming Mars Exploration Rover Pancam investigation (Bell et al., 2003); and (3) determine whether mafic silicate ± palagonitic material assemblage properties, such as end member abundances, compositions, and grain sizes, can be quantified or constrained using this lower spectral resolution data. This study extends the work done on analysis of Pathfinder IMP data for constraining the nature of Mars surface materials at the Pathfinder site (e.g., McSween et al., 1999; Bell et al., 2000; Morris et al., 2000) by examining in more detail mafic silicates ± palagonitic material and terrestrial ferric iron-bearing minerals.

2. Experimental procedure

In order to understand the spectrum-altering effects of palagonitic material on mafic silicates, a series of intimate mixtures of orthopyroxene + palagonitic material and orthopyroxene + hematite were spectrally characterized. We retain the convention of referring to low-calcium pyroxenes as orthopyroxenes and high-calcium pyroxenes as clinopyroxenes, even though some low-calcium pyroxenes may have a monoclinic rather than orthorhombic structure. A representative orthopyroxene (PYX110, Table 1) was used to produce intimate mixtures with palagonitic material or hematite. This pyroxene was used because it is spectrally most similar to martian meteorite pyroxenes in

Table 1
Compositions of the main samples used in this study

wt%	PYX110	PAL101[a]	PAL102[b]
SiO_2	56.65	41.24	45.5
Al_2O_3	0.03	25	18.4
FeO	9.19	2.77	
Fe_2O_3	0.44	12.58	13.1[c]
MgO	33.92	3.52	3.91
CaO	0.30	5.11	6.02
Na_2O	0.00	2.74	3.24
TiO_2	0.03		3.24
Cr_2O_3	0.05	0.01	
V_2O_5	0.01	0.02	
CoO	0.01		
NiO	0.02		
MnO	0.04	0.29	0.22
K_2O		0.67	1.07
P_2O_5		1.34	0.59
LOI[d]		13.89	4.77
Total	100.69	99.19	100.4

[a] analysis of 5–53 µm size fraction from Morris et al. (2000).
[b] analysis of < 2 mm size fraction from Banin et al. (1997).
[c] All Fe reported as Fe_2O_3.
[d] loss on ignition. Sample PAL101 was heated in air at 950 °C for one hour and samples PAL102 was heated to 950 °C for an unknown period of time to determine volatile content.

Table 2
End member abundances and grain sizes of minerals used to generate intimate mixtures

Sample No.	PYX110		PAL101		PAL102		HEM101	
	Size (µm)	wt%	Size (µm)	wt%	Size (µm)	wt%	Size (µm)	wt%
MIX501	45–90	90	< 45	10				
MIX502	45–90	80	< 45	20				
MIX503	45–90	70	< 45	30				
MIX504	45–90	60	< 45	40				
MIX505	45–90	50	< 45	50				
MIX506	45–90	40	< 45	60				
MIX507	45–90	30	< 45	70				
MIX508	45–90	20	< 45	80				
MIX509	45–90	10	< 45	90				
MIX510	< 45	80	< 45	20				
MIX511	< 45	60	< 45	40				
MIX512	< 45	40	< 45	60				
MIX515	45–90	80			< 45	20		
MIX516	45–90	60			< 45	40		
MIX517	45–90	80					< 0.14	20
MIX518	45–90	60					< 0.14	40

See Table 1 for composition of the end members. PYX110 = orthopyroxene; PAL101, PAL102 = palagonite; HEM101 = hematite.

the 300- to 800-nm region (Salisbury et al., 1975; Gaffey, 1976; McFadden, 1987; Wagner et al., 1987; Morris, 1989; Sunshine et al., 1993; Schade and Wäsch, 1999). It was characterized compositionally and structurally (Cloutis and Gaffey, 1991a) and was found to be free of any contaminating weathered phases. Palagonitic material samples were kindly made available by Dick Morris at JSC (sample number HWMK 600; PAL101 in this study) (Morris et al., 2000) and Ted Roush at NASA Ames Research Center (sample number 91-16; PAL102 in this study) (Banin et al., 1997). Dick Morris also provided the synthetic hematite sample used in this study (sample number HMS3; HEM101 in this study) (Morris et al., 1985). The palagonitic material samples were dry sieved, without crushing, to obtain a < 45 µm fraction. The pyroxene sample was crushed in an alumina mortar and pestle and dry sieved to produce the various powdered size fractions.

The various samples were characterized by X-ray diffraction at the University of Manitoba. Continuous scan X-ray diffraction data were collected from 3°–65° 2-θ on a Philips PW1710 automated powder diffractometer, using a PW1050 Bragg-Brentano goniometer equipped with incident- and diffracted-beam Soller slits, 1.0° divergence and anti-scatter slits, a 0.2 mm receiving slit and a curved graphite diffracted-beam monochromator. The normal focus Cu X-ray tube was operated at 40 kV and 40 mA, using a take-off angle of 6°. The pyroxene XRD trace showed only pyroxene peaks, while the palagonitic material XRD traces showed a few broad diffuse peaks which could not be uniquely assigned with any confidence to any particular mineral phases; the closest match being to plagioclase feldspar.

Reflectance spectra were acquired at the NASA-supported RELAB spectrometer facility at Brown University (Pieters, 1983; RELAB, 1996). Reflectance spectra were measured from 0.3- to 2.6-µm at 5 nm spectral resolution with $i = 30°$ and $e = 0°$, and were measured relative to halon The spectra were acquired under dry air conditions. Heating of the palagonitic material samples was undertaken in air and the samples were placed in sealed containers immediately after heating and weighing, and kept in these containers until they were spectrally characterized. It is likely that the samples adsorbed some moisture from the atmosphere during the short times that they were out of their containers. Thus, the absorption bands seen in the 1.4- and 1.9-µm regions are likely due to a combination of structural water and adsorbed water, as spectral measurements under dry air measurement conditions probably did not liberate all the adsorbed water. We intend to remeasure these samples under Mars surface conditions in the future.

Intimate mixtures of PYX110 and palagonitic material or hematite were prepared at various wt% intervals for spectral measurements (Table 2). Equivalent areal mixtures were generated by applying appropriate weighting factors to the end member spectra in an additive (linear) fashion. As an example, a 20/80 areal mixture of pyroxene + palagonitic material would be the sum of 0.2 times the pyroxene spectrum plus 0.8 times the palagonitic material spectrum. Band depths (D_b) for the high-spectral resolution data were measured using Eq. (32) of Clark and Roush (1984). Band depths for the broad-band data were measured using the same relationship. For the Pathfinder data, the continua for the 931 and 531 nm "bands" were straight lines connecting the 858 and 1003 nm, and the 480 and 600 nm data points, respectively; for the HST data, the continua for the 955 and 501 nm "bands" were straight lines connecting the 860 and 1044 nm,

and the 409 and 673 nm data points, respectively. Band minima for the high resolution data were determined by fitting a third order polynomial to between 10 and 20 data points on either side of a visually determined band minimum. Changing the number of data points used for band minimum determination caused band minimum positions to vary by less than ± 2 nm. The spectra used in this study were augmented by additional spectra available in the literature for mafic silicates, mafic silicate-bearing mixtures, Mars Pathfinder and telescopic Mars spectra, and various ferric iron-bearing oxides and hydroxides. Band widths (full width half maxima (FWHM)) are the width, in nanometers, at half the depth of the band after removal of a straight line continuum.

3. Palagonitic material as a martian bright region or "dust" spectral analog

Analysis of pyroxene reflectance spectra for deriving compositional information is most robust when both the 1000 nm and 2000 nm region absorption bands (commonly referred to as Band I and Band II regions, respectively) are available (Adams, 1974; Cloutis et al., 1986; Cloutis and Gaffey, 1991a). Palagonitic materials, containing nanophase iron oxides as a pigmenting agent, are spectrally similar to martian bright region spectra and serve as a spectral (and perhaps compositional) analog for martian fines at wavelengths below $\sim$ 1000 nm (e.g., Morris et al., 1989, 1993; Bell et al., 1993; Golden et al., 1993; Morris and Golden, 1998). Both the PAL101 and PAL102 samples are suitable spectral analogues for the shorter wavelength portions of martian bright region spectra and both are spectrally similar (Fig. 1). Both sample spectra exhibit H_2O/OH-associated absorption features in the 1400 and 1900 nm regions. Such bands are weak or non-existent in martian surface spectra (Murchie et al., 1993).

Attempts to remove or diminish the intensities of the 1400 and 1900 nm region bands from the palagonitic material spectra by heating the samples (to 160 and 600 °C for 2 hours) were unsuccessful and produced other undesirable spectral changes (Fig. 1), probably due to recrystallization, incomplete dehydration, and resorption of atmospheric moisture, similar to the results found by Bruckenthal (1987). Many of the spectral changes accompanying heating are similar to those found in a naturally thermally altered palagonitic tephra (Bell et al., 1993). X-ray diffractograms of the heated and unheated samples showed no significant differences in terms of the appearance of new diffraction peaks; the only noticeable changes accompanying heating were reductions in the FWHM of some of the broad and diffuse peaks. The only mineral phase that could be identified with certainty in all of the diffractograms was plagioclase feldspar.

Total weight losses upon heating were 9.6 and 6.7 wt% for PAL101 and PAL102 heated to 160 °C, respectively, and 16.4 and 14.8% for the same samples heated to 600 °C.

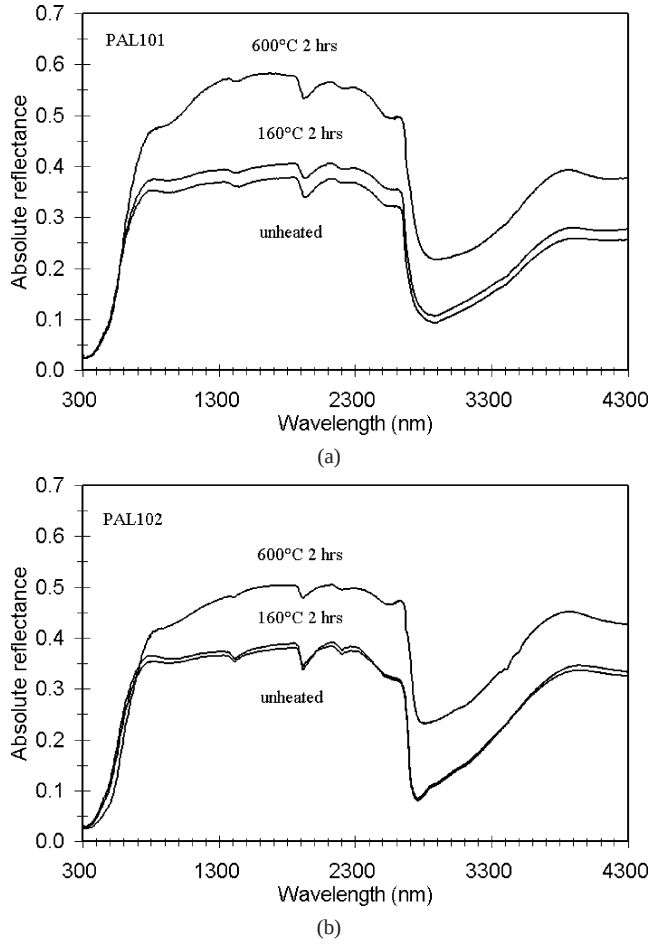

Fig. 1. 300–4300 nm reflectance spectra of palagonitic material samples PAL101 (a) and PAL102 (b), unheated and heated in air to 160 and 600 °C for 2 hours. See Table 1 for compositional information.

These values exceed those measured by the original investigators, likely due to the fact that volatiles are expected to be concentrated in the finer fractions; volatile content measurements for the original samples involved larger grain size fractions than those used here (Table 1). The < 45 μm fractions of both samples exhibit overall reflectance in the 1000 nm region that is similar in both shape and absolute value to the martian bright regions, as well as to some Pathfinder bright soil spectra; absolute reflectance of these martian spectra generally range from ~ 0.3 to ~ 0.4 at 800 nm (Murchie et al., 1993; Bell, 1996; Bell et al., 1997, 2000; McSween et al., 1999), while the palagonitic material spectra have absolute reflectance of 0.35–0.37 at this wavelength.

Due to the persistence of a 1900 nm feature in the palagonitic material spectra, the 2000 nm region of the pyroxene + palagonitic material mixture spectra was not used for derivation of spectral-assemblage property relationships. However mafic silicate compositions can be derived solely from the 1000 nm absorption feature (Cloutis and Gaffey, 1991a, 1991b), so omission of the 2000 nm region at this stage is not a significant impediment to analysis of mafic

silicate-bearing assemblages. In addition, while palagonitic material may be a reasonable spectral analogue for martian fines, it would be useful to have a better understanding of the optical properties of this material, as even spectrally "neutral" components can affect band area ratios (Moroz and Arnold, 1999).

4. Pyroxene + palagonitic material mixture spectra

Pyroxene + palagonitic material mixtures were produced at 10 wt% intervals for the main series involving 45–90 μm fractions of pyroxene (PYX110) and < 45 μm fractions of palagonitic material (PAL101), as both intimate and areal mixtures as described above (Fig. 2). This was designed to simulate expected differences in grain size between the finer-grained martian "dust" (Pollack et al., 1977; Clancy et al., 1995) and coarser-grained martian pyroxene (McSween and Treiman, 1998). Additional, but more limited, series were produced using a smaller grain size of PYX110 (< 45 μm) with PAL101, and 45–90 μm sized PYX110 with PAL102 and hematite (HEM101) (Table 2).

Quantitative analysis of reflectance spectra to derive compositional information for pyroxenes and other mafic silicates is based on absorption band wavelength positions for major element composition (Cloutis and Gaffey, 1991a), and band depths for the coupled effects of grain size and relative abundance in the presence of other phases (Cloutis et al., 1986). In cases where absolute reflectance values are known, grain size and relative abundance effects may be partially resolvable.

The wavelength position of the pyroxene Band I center varies between 911 and 914 nm for all of the intimate mixture series (10–100 wt% pyroxene) with no systematic trends apparent. The areal mixture series exhibits absorption band center positions between 912 and 916 nm, with a small (1–2 nm) increase in band position for those samples containing > 80 wt% palagonitic material. This slight increase in band position at high palagonite abundances is due to the fact that the palagonitic materials used in this study both exhibit a weak (D_b = 2–3%) absorption feature located at 926 nm (PAL101) or 958 nm (PAL102). The range of band position variations is less than the spectral resolution of the laboratory data (5 nm) and much less than the variations in band positions associated with pyroxene compositional changes (> 100 nm for Band I) (Cloutis and Gaffey, 1991a).

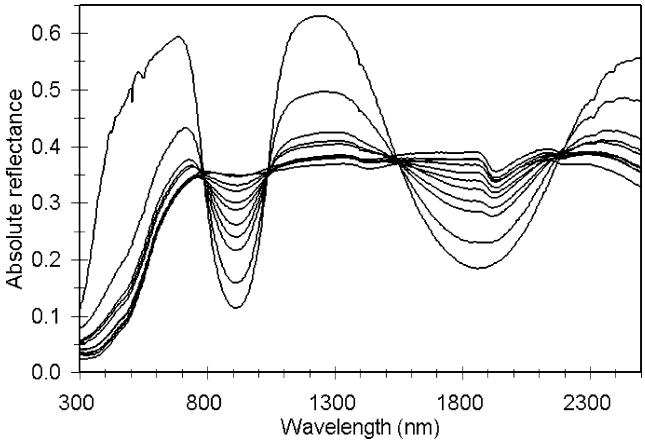

Fig. 2. Reflectance spectra of 10 wt% interval intimate mixtures of orthopyroxene (PYX110, 45–90 μm grain size) and palagonitic material (PAL101, < 45 μm grain size). wt% palagonitic material increases with decreasing band depth in the 900 and 1900 nm regions.

Full width half-maxima (FWHM) values of Band I have been found to be relatively constant for orthopyroxene-clinopyroxene mixture series (Sunshine and Pieters, 1993). In our study, where the orthopyroxene has a band width of either 200 (for the < 45 μm size fraction) or 250 nm (for the 45–90 μm size fraction), and the palagonitic material has a band width of 225 nm for PAL101 and 240 nm for PAL102, decreases in band width were generally found for decreasing pyroxene content for all pyroxene abundance for both the intimate and areal mixture series; the only major exception being the pure palagonitic materials (Fig. 3). This is consistent with the behavior associated with dilution of a spectrally featured material mixed with a relatively spectrally neutral, and bright, component (Cloutis and Bell, 2000). It was also found that the FWHM is a function of pyroxene composition. FWHM of < 45 and 45–90 μm size samples of the orthopyroxenes from Cloutis and Gaffey (1991a) range from 190–270 nm; the range for clinopyroxenes is slightly larger: 180–297 nm. Since FWHM is also a function of pyroxene grain size and palagonitic material abundance, it cannot be used in isolation to uniquely constrain pyroxene composition, abundance, or grain size.

Band depths for the orthopyroxene + palagonitic material spectra (Fig. 4) converge rapidly to a single trend for the intimate mixture series, while the areal series show more scatter. The trends are as expected because fines will dominate the spectral properties. This kind of mixture is often non-linear for greatly different particle sizes. Band depths for the Cloutis and Gaffey (1991a) orthopyroxenes range from 47 to 82%, close to the range of the single pyroxene used in the intimate mixtures. The fact that the band depth values for the palagonitic material-bearing series rapidly converge to a single trend with decreasing pyroxene abundance suggests that band depths can be used to constrain orthopyroxene abundances across a range of compositions and grain sizes, assuming that pyroxene and palagonitic material are (optically) intimately mixed and are the spectrally dominant phases. Terrestrial clinopyroxenes are more spectrally diverse than martian pyroxenes (e.g., Adams, 1974, 1975; Cloutis, 1985; Morris, 1989, Cloutis and Gaffey, 1991a, 1991b; Morris et al., 2000), largely as a result of greater compositional variations and the presence of appreciable amounts of ferric iron in many terrestrial clinopyroxenes, which has its major effect at shorter wavelengths ($\lesssim$ 1000 nm); this results in clinopyroxene Band I depths ranging between 3 and 74% for all the available terrestrial samples used in this study. The data shown in Fig. 4

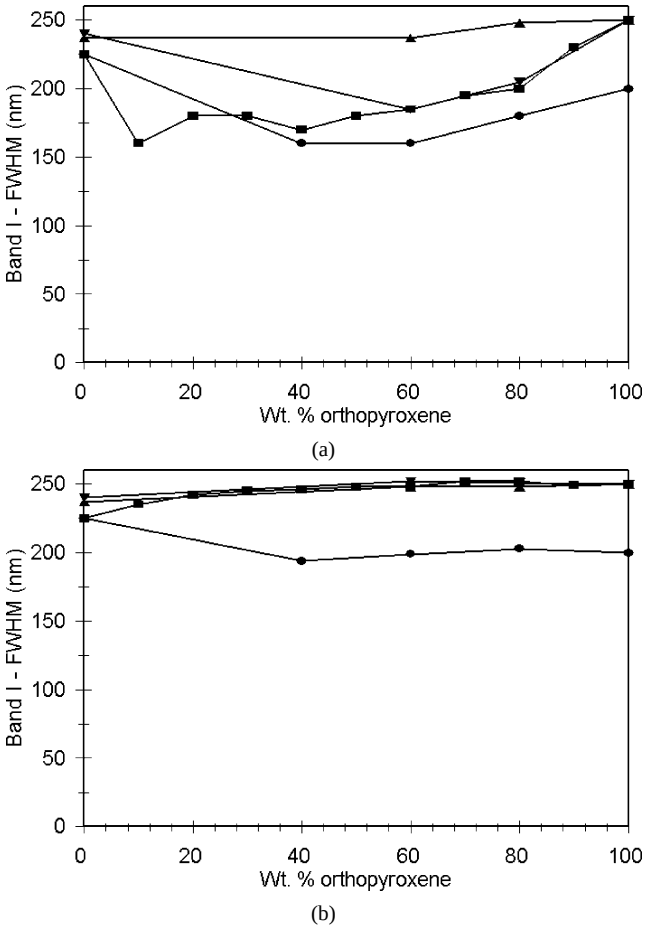

Fig. 3. Variation in full width half maxima of the Band I feature in the intimate (a) and areal (b) mixtures of orthopyroxene (PYX110, < 45 and 45–90 μm grain sizes) and palagonitic material (PAL101, < 45 μm grain size; PAL102, < 45 μm grain size) or hematite (HEM101, < 140 nm grain size). ■—PYX110 (45–90 μm) + PAL101; ●—PYX110 (45–90 μm) + PAL102; ▼—PYX110 (< 45 μm) + PAL101; ▲—PYX110 (45–90 μm) + HEM101. End member abundances are provided in Table 2. Interpolating values between points separated by more than 20 wt% orthopyroxene may not be valid.

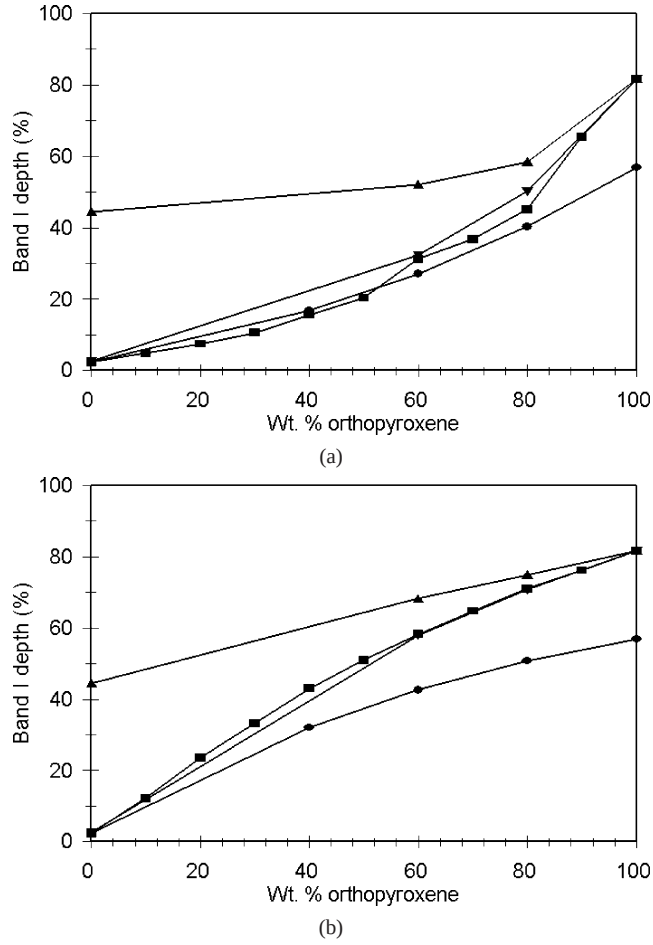

Fig. 4. Variations in depth of the Band I feature in the intimate (a) and areal (b) mixtures of orthopyroxene (PYX110) and palagonitic material (PAL101, PAL102) or hematite (HEM101). Symbols are the same as those in Fig. 3. Interpolating values between points separated by more than 20 wt% orthopyroxene may not be valid.

can be used to place a lower limit on pyroxene abundance given the fact that the pyroxene used in this study (PYX110) exhibits the largest band depth of all the pyroxenes examined.

4.1. Systematic spectral variations

Analysis of martian reflectance spectra for pyroxene mapping would ideally provide information on pyroxene composition, abundance, and grain size. Under the assumption that a material spectrally similar to palagonitic material is the major spectrally-dominant accessory phase, the results of this study suggest that pyroxene composition should be derivable from the position of Band I (Cloutis and Gaffey, 1991a), since it is relatively unaffected by the presence of palagonitic material (up to 90 wt% palagonitic material) in either intimate or areal mixtures. Additional constraints could be placed on pyroxene abundance through the use of Band I depth determinations, if intimate mixing with palagonitic material is assumed (Mustard et al., 1993a; Mustard and Sunshine, 1995).

The relative constancy of the pyroxene Band I wavelength position at palagonitic material abundances up to 90 wt% is related to the decreasing optical density of palagonitic material with increasing wavelength and the relatively flat slope of palagonitic material in the 1000 nm region (Singer and Roush, 1983). Palagonitic material more strongly affects spectral properties at progressively shorter wavelengths, when palagonitic material is present as either a surface coating or intimately mixed with other materials (e.g., Singer and Roush, 1983; Morris et al., 1997; Johnson and Grundy, 2000). A similar invariance in band positions for features near 1000 nm is also seen in many naturally weathered basalts (Singer, 1980; Pieters, 1989). These results collectively suggest that where mafic silicate bands are resolvable, their wavelength position can be used to constrain mafic silicate composition (Cloutis et al., 1986; King and Ridley, 1987; Cloutis and Gaffey, 1991b).

Complications in deriving mafic silicate compositions from absorption band positions will arise when other minerals with absorption bands in the same wavelength region are present. This appears to be the case for at least some of the Pathfinder IMP spectra (Bell et al., 2000; Morris et al., 2000). Possible candidate minerals identified by Morris et al. (2000) that possess an absorption feature near 930 nm (and which could affect mafic silicate compositional determinations) include nanophase goethite, maghemite, akagenite, and schwertmannite. The possible complications introduced by the presence of such a material on the interpretation of rock type diversity at the Pathfinder site has been described by Yingst and Smith (2000). The ability to discriminate spectral variations associated with mafic silicate compositional variations as opposed to palagonitic material abundance variations is discussed more fully below.

Band depths and widths did not appear to be strongly correlated with composition for either orthopyroxenes or clinopyroxenes. The available data suggest that band depths and widths increase with increasing iron and calcium contents, however, grain size variations are the dominant factor controlling these spectral parameters (Sunshine and Pieters, 1993; Cooper and Mustard, 1999). Therefore, absorption band wavelength position remains the most reliable method for determining pyroxene chemistry even in the presence of palagonitic material. If a more accurate spectral analogue of martian fines beyond 1200 nm is identified, in terms of showing no resolvable water-associated absorption bands, interpretation of reflectance spectra to 2500 nm may allow a more comprehensive and robust interpretation of mafic silicates + martian fines to be undertaken (e.g., Cloutis et al., 1986; Cloutis and Gaffey, 1991b).

The results for our intimate mixtures of pyroxene + palagonitic material are broadly consistent with the results of previous investigations. Palagonitic material is increasingly transparent at longer wavelengths and mafic silicate absorption band positions are largely unaffected by the presence of palagonitic material coatings until the coatings are thick enough to obscure the mafic silicate absorption bands (e.g., Singer and Roush, 1983; Pieters, 1989; Johnson and Grundy, 2000; Morris et al., 2001b). The major difference between the intimate mixtures and palagonitic material-coated materials is that the palagonitic material-coated sample spectra generally show negative spectral slopes while the intimate mixture spectra do not (Fig. 2).

5. Effects of degraded spectral resolution

To date, most VIS-NIR spectral reflectance-based mapping of the martian surface has involved either high spectral resolution for limited areas (e.g., Mariner 6, 7 IRS, Phobos ISM) or low spectral resolution for larger regions (e.g., Viking Orbiter, Mars Odyssey THEMIS/VIS). We examined the quantity of information derivable from analysis of multispectral data for mapping of mafic silicate geological variations by degrading the spectral resolution of laboratory reflectance spectra of mafic silicates, ferric iron-bearing oxides and hydroxides, mixtures of these phases, pyroxene + palagonitic material mixtures, Marts meteorites, and Earth-based Mars telescopic spectra; approximately 700 spectra were used in the analysis. The specific band passes that were chosen were those used for recent global mapping of Mars with the WFPC2 on the Hubble Space Telescope (Bell et al., 1997), and the imager on Mars Pathfinder (Smith et al., 1997) (Table 3). The general approach outlined here should be applicable to any multispectral observations in which absorption features are represented by only a few data points and for limited wavelength coverage. Compositionally diagnostic spectral properties of mafic silicates, such as absorption band wavelength positions or band widths will generally not be obtainable with a high degree of precision from multispectral data. Ideally, we would like to analyze such spectra to derive composition, grain sizes, and end member abundances for mafic silicates and any accessory phases.

The mafic silicate mineralogy of Mars, inferred from SNC meteorites, consists largely of orthopyroxene, clinopyroxene, and olivine, with lesser amounts of other minerals (McSween and Treiman, 1998). This is consistent with spectroscopic studies of Mars, particularly in the dark regions (Soderblom, 1992; Mustard et al., 1993a; Roush et al., 1993; Bell, 1996; Christensen et al., 1998, 2000). Therefore, we focused on the spectral variations accompanying changes in end member abundances, grain sizes, and major element compositions of these materials.

5.1. Spectral trends for individual mineral parameters

An examination of the spectral properties of pure phases and mixtures involving orthopyroxene, clinopyroxene, olivine, and palagonitic material degraded to the bandpasses of a recent HST observational campaign and Pathfinder IMP (Table 3; Fig. 5) failed to reveal a full suite of unique sys-

Table 3
Band centers and full width half maxima of HST WFPC2 observations by Bell et al. (1997) and of Pathfinder IMP (Smith et al., 1997)

HST WFPC2		Pathfinder IMP		
Center wavelength, nm	Full width half maximum, nm	Filter	Center wavelength, nm	Full width half maximum, nm
256	41	L0, R0	443.3	26.2
333	37	R10	479.9	27.0
409	15	R9	530.8	29.6
501	3	R8	599.5	21.0
673	5	R5	671.2	19.5
740	10	L5	671.4	19.7
860	11	R6	752.0	18.9
955	5	L6	801.6	21.0
1044	61	L7	858.4	34.4
		L8	897.9	40.8
		L9	931.1	27.0
		R11	966.8	29.6
		L11	968.0	31.4
		L10	1002.9	29.1

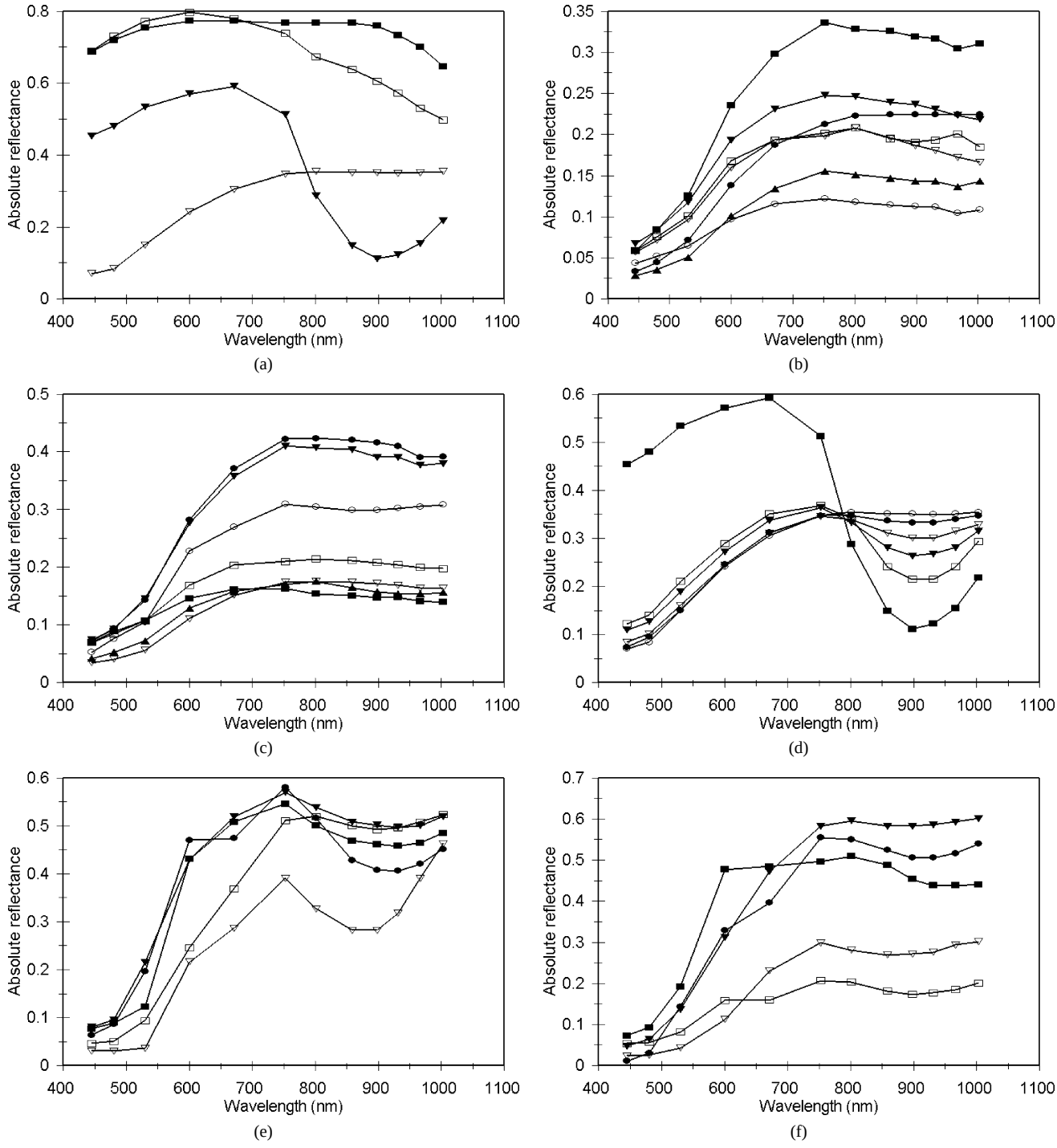

Fig. 5. Reflectance spectra of various mineral and mixture spectra deconvolved to Pathfinder IMP band passes. (a) Clinopyroxene (this study; < 45 μm) [■], olivine (this study; < 45 μm) [□], orthopyroxene (PYX110; 45–90 μm) [▼], and palagonitic material (PAL101; < 45 μm) [▽]. (b) Pathfinder soils from Bell et al. (2000): Bright I soil spectrum 19-1 [■], Bright II soil spectrum 36-1 [□], Bright III soil spectrum 58-1 [▼], Bright IV soil spectrum 07-1 [▽], Surface Dust spectrum 21-2 [●], Dark soil spectrum 21-1 [○], Disturbed soil spectrum 47-2 [▲]. (c) Pathfinder rock spectra from McSween et al. (1999): Booboo [■], Half Dome [□], Scooby Doo [▼], Valentine [▽], Baker's Bench [●], and telescopic spectra from Bell (1996): Bright region 88-41 spectrum [○], Dark region 88-22 spectrum [▲]. (d) Pyroxene + palagonitic material series from Table 2: PYX110 (45–90 μm grain size) [■], MIX502 [□], MIX504 [▼], MIX506 [▽], MIX508 [●], PAL101 [○]. (e) iron-bearing oxides and hydroxides: akagenite (sample SAK1 from Morris et al. (2000); < 90 μm) [■], maghemite (sample LPS2-3-265 from Morris et al. (2000); < 90 μm) [□], schwertmannite (sample BT-4 from Morris et al. (2000); < 90 μm) [▼], hematite (this study; < 45 μm) [▽], jarosite (this study; < 45 μm) [●]. (f) iron-bearing oxides and hydroxides: lepidocrocite (sample LPS2 from Morris et al. (2000); < 90 μm) [■], goethite (this study; < 45 μm) [□], ferrihydrite (sample H3 from Morris et al. (2000); < 90 μm) [▼], ferroxyhyte (synthetic sample delta-1 from Sherman et al. (1982); < 1.5 μm) [▽], limonite (sample Lim41 (< 74 μm) from Hunt et al. (1971)) [●].

tematic spectral trends that could be used to quantify all possible combinations of mineralogical factors for mafic silicate + palagonitic material mixtures (i.e., end member abundances, grain sizes, and compositions). This is due to the natural spectral variability of some of these phases, particularly clinopyroxenes, as well as the coarse spectral resolution of the data, which precludes precise determination of absorption band minima. It is worth noting that the mafic silicates (Fig. 5a) all exhibit relatively flat spectra in the 0.4- to 0.7-μm interval, while all the Mars surface and telescopic spectra, ferric iron-bearing sample and pyroxene + palagonitic material mixture spectra all exhibit red slopes in this region.

Based on previous work involving the spectral properties of palagonitic materials and other basaltic weathering products, it has been found that basaltic alteration products most strongly affect the wavelength region below ∼ 800 nm (Singer and Roush, 1983; Pieters, 1989; Morris et al., 2001b). In the case of mafic silicates plus iron oxides, ferric coatings on basalt experiments (Fischer and Pieters, 1993) indicate that increases in the thickness of the ferric coating (on basalt) lead to decreases in reflectance ratios of bands below ∼ 700 nm ratioed to longer wavelength bands (> 750 nm). As an example, the 600/1003 nm reflectance ratio of a ferric coated basalt decreases from 0.792 for a 4-μm thick coating to 0.633 for a 225-μm thick coating (20% decrease). However, the 750/1003 nm reflectance ratio only differs by 8% between these two samples. This supports the contention that ferric iron-bearing coatings of fine particles have their greatest impact at $\lesssim$ 750 nm. With increasing wavelength, the optical density of palagonitic material decreases and mafic silicate absorption features become increasingly apparent. Given these observations and the fact that the 1000 nm region is more useful for compositional determinations in mafic silicates than lower wavelengths, we focused on the bandpasses longward of 800 nm for their ability to provide information concerning the mafic silicates, and the bands shortward of 800 nm for their ability to constrain ferric iron-bearing phase abundances.

Ratios of reflectance values involving the various band passes provide the most diagnostic information because reflectance ratios, at least for mafic silicates, appear to be relatively insensitive to modest variations in viewing geometry (Pieters, 1983). As an example, the 600/1003 nm reflectance ratio of olivine is 2.11 for $i = 45°$ and $e = 60°$ (15° phase angle) and 1.96 for $i = 35°$ and $e = -60°$ (95° phase angle), a difference of ∼ 7% (Mustard and Pieters, 1989).

In the case of ferric coatings on basalt (Fischer and Pieters, 1993), viewing geometry variably affects reflectance ratios in a wavelength-dependent manner. For 225-μm thick ferric coatings on basalt, the 600/1003 and 750/1003 nm reflectance ratios vary by < 3% when the phase angle varies between 30° and 90°. For a thinner coating (4-μm), the situation is more complex: the 600/1003 and 750/1003 nm reflectance ratios vary by up to 50 and 3%, respectively, for phase angle ranges of 15° to 60°. Viewing geometry effects have been invoked to account for spectral differences in Pathfinder rock spectra (Yingst and Smith, 2000). Collectively, these results suggest that viewing geometry effects will be most important for shorter wavelength regions, but that determinations involving longer wavelength bands will be minimally affected by modest variations (a few tens of degrees) in viewing geometry.

Changes in all the possible reflectance ratios of all the available bands were examined relative to changes in both end member abundances and compositions for pure and mixed end member mafic silicates, the orthopyroxene + palagonitic material mixtures, and various ferric iron-bearing phases. These were augmented by various measures of band depths involving three band passes (e.g., Morris et al., 2000). The spectral trends which were found are summarized in Table 4 and are discussed in more detail below. Over 700 spectra were used in the analysis from a variety of sources (see Table 4 for data sources which augmented the data generated for this study).

Prior to the ensuing discussion it should be emphasized that many of the reflectance ratios can be affected by changes in more than one assemblage property. As an example, the 1044/955 nm reflectance ratio (Table 4) is a function of palagonite abundance, orthopyroxene, clinopyroxene and olivine ferrous iron contents, orthopyroxene and olivine grain sizes, pyroxene calcium content, and clinopyroxene and olivine abundances (in the presence of orthopyroxene). Consequently attempting to use this spectral parameter to quantify any of these assemblage properties cannot yield a unique solution. The best that can be derived is to determine relative changes in target properties, and even this approach requires the application of multiple spectral parameters to provide a constrained solution. For this reason, uncertainties inherent in the use of the spectral parameters for quantifying assemblage in Table 4 cannot be assigned.

5.1.1. Palagonitic material abundance variations

The spectral properties of palagonitic material at wavelengths shorter than ∼ 800 nm are most strongly affected by their included ferric iron-bearing compounds (Morris et al., 1993, 1997; Morris and Golden, 1998). As a result, this wavelength region was found to be most diagnostic for determining palagonitic material abundances in mafic silicate + palagonitic material mixtures. Of the various reflectance ratios examined, the 740/501 nm (for HST) and 752/480 nm (for IMP) reflectance ratios were found to be most sensitive to palagonitic material abundance. This value ranges from 1.3 to 10.2 for the 740/501 nm ratio and from 1.4 to 10.6 for the 752/480 nm ratio, for the < 45 μm palagonitic material separates, Pathfinder bright soil spectra, and Mars bright and dark region spectra (Singer, 1985, Bell et al., 1990, 2000; Soderblom, 1992; Roush et al., 1993; Bell, 1996; McSween et al., 1999; Morris et al., 2000) (Table 5). Palagonitic materials most similar to Mars bright region spectra have 740/501 nm and 752/480 nm ratios of 3.0–3.2 and 3.5–4.1, respectively (Fig. 6). Values above 4.1

Table 4
Summary of systematic spectral variations for mafic silicates and palagonitic material

Petrologic variable (increasing)	Reflectance ratio (values in nm)							
HST								
	740/501	860/955	1044/955	860/1044	740/955	740/1044	740/860	
PAL content	+	n.t.	→ 1	→ 1	→ 1	→ 1	→ 1	
OPX Fe^{2+} content	n.c.	+	−	n.t.	n.t.	n.t.	n.t.	
OPX grain size	n.c.	n.t.	+	−	+	+	+	
CPX grain size	n.c.	+	n.c.	+	+	+	n.t.	
CPX Fe^{2+} content	n.t.	n.t.	+	−	+	n.t.	n.t.	
PYX Ca content	n.c.	n.t.	−	+	−	n.t.	n.t.	
CPX content (+OPX)	n.t.	+	−	+	−	n.t.	−	
OLV grain size	n.t.	+	−	+	+	+	+	
OLV Fe^{2+} content	+	n.t.	+	−	n.t.	n.t.	−	
OLV content (+CPX)	−	−	n.t.	−	n.t.	n.t.	−	
OLV content (+OPX)	n.t.	n.t.	−	+	−	+	−	
Pathfinder IMP								
	752/480	1003/931	1003/967	858/1003	752/967	752/1003	752/858	858/967
PAL content	+	→ 1	→ 1	→ 1	→ 1	→ 1	→ 1	n.t.
OPX Fe^{2+} content	n.t.	−	−	n.t.	n.t.	n.t.	n.t.	+
OPX grain size	n.t.	+	+	−	+	+	+	n.t.
CPX grain size	n.t.	−	n.c.	+	+	+	n.t.	+
CPX Fe^{2+} content	n.t.	+	+	−	+	n.t.	n.t.	n.t.
PYX Ca content	n.t.	−	−	+	−	n.t.	n.t.	n.t.
CPX content (+OPX)	n.t.	−	−	+	−	n.t.	−	+
OLV grain size	n.t.	−	−	+	+	+	+	+
OLV Fe^{2+} content	+	+	+	−	n.t.	n.t.	−	n.t.
OLV content (+CPX)	n.a.	n.t.	n.t.	−	+	+	+	n.t.
OLV content (+OPX)	n.t.	−	−	+	n.t.	n.t.	n.t.	n.t.

+—reflectance ratio increases with increase in petrologic variable; −—reflectance ratio decreases with increase in petrologic variable; → 1—approaches a value of 1; n.t.—no systematic trend; n.c.—no or minor change; n.a.—not available (insufficient data to establish a trend). OPX—orthopyroxene; CPX—clinopyroxene; OLV—olivine; PAL—palagonitic material; PYX—pyroxene (orthopyroxene and clinopyroxene).
Sources of data: this study; Hunt et al., 1971, 1973; Gaffey, 1974; Adams et al., 1979, 1986; Gaffey and McCord, 1979; King et al., 1981; Miyamoto et al., 1981; Sherman et al., 1982; Miyamoto et al., 1983; Morris et al., 1983, 1985, 1986, 1989; Hiroi et al., 1985; Singer, 1985; Crown and Pieters, 1987; King and Ridley, 1987; Mustard and Pieters, 1987, 1989; Roush et al., 1987; Wagner et al., 1987; Azuma and Fujii, 1989; Bartels and Burns, 1989; Hiroi and Takeda, 1989; Taranik and Kruse, 1989; Bell et al., 1990, 1993, 2000; Clark et al., 1990; Kinoshita and Miyamoto, 1990; Morris and Lauer, 1990; Sunshine et al., 1990; Besancon et al., 1991; Cloutis and Gaffey, 1991a, and references therein; Farrand and Singer, 1991; Straub et al., 1991; Grove et al., 1992; Johnson et al., 1992; Allen et al., 1993; Golden et al., 1993; Mustard et al., 1993b; Sunshine and Pieters, 1993, 1998; Sunshine et al., 1993; Hiroi and Pieters, 1994; Bishop and Pieters, 1995; Bell, 1996; Bishop and Murad, 1996; Mustard and Hays, 1997; Lucey, 1998; Bishop et al., 1998a, 2001; Buemi et al., 1998; McSween et al., 1999; Schade and Wäsch, 1999; Morris et al., 2000, 2001a.

were found for some of the Pathfinder soil and rock spectra and some Mars bright region telescopic spectra (e.g., Bell, 1996) and most pure ferric iron-bearing minerals (Table 5); this indicates that the palagonitic material samples used as spectral analogues for telescopic spectra of martian bright regions may not be appropriate for simulating the spectral properties of all occurrences of dust at small (landing site) scales. However, it should be noted that both Mars bright region spectra and volcanic alteration products are highly variable in composition and spectral properties (Bell et al., 1990); consequently, the full range of possible spectral variability of Mars is under-represented here.

The magnitude of these reflectance ratios decreases in the laboratory spectra with increasing mafic silicate abundance, regardless of mafic silicate grain size, type, and composition, ranging between ∼ 0.7 and 1.7 (740/501 nm) and between ∼ 0.6 and 2.0 (752/480 nm) for all terrestrial mafic silicates, martian meteorites, and a few of the Pathfinder rock spectra (Fig. 6). These ratios are also lower for Mars dark region spectra than bright region spectra, consistent with the interpretation that the dark regions are more dust-free (e.g., Singer, 1985; Soderblom, 1992; Roush et al., 1993).

When the short wavelength reflectance ratios are plotted against a reflectance ratio based on longer wavelength bands (which should be less affected by the presence of palagonitic material), such as the 1044/955 nm versus 740/501 nm ratios (Fig. 6a), and 1003/931 nm versus 752/480 nm ratios (Fig. 6b), the presence of as little as 10 wt% palagonitic material intimately mixed with mafic silicates shifts the 740/501 or 752/480 nm reflectance ratios outside of the field of the pure mafic silicates and Mars meteorites. Thus the 740/501 or 752/480 nm reflectance ratios can be used to detect the presence of palagonitic material (or spectral equivalent) and constrain its abundance (Fig. 6, Table 4). Increasing palagonitic material abundance causes the 740/501 and 752/480 nm reflectance ratios to shift to higher values. The reflectance ratios involving any combina-

Table 5
Reflectance ratios for Pathfinder, telescopic spectra, and ferric iron-bearing minerals

Category	740/501 nm ratio	752/480 nm ratio	Source of data
Pathfinder soils	n.a.	2.3–6.0	1
Pathfinder rocks	n.a.	1.8–4.5	2
Mars bright regions	3.2–3.6	3.6–4.4	3, 4, 5
Mars intermediate regions	2.5–3.4	2.8–3.9	5
Mars dark regions	2.0–2.7	2.3–3.1	3, 4, 5
Akagenite	6.4–7.5	6.1–8.1	6, 7
Maghemite	2.4–11.5	2.4–15.6	6–9
Schwertmannite	4.9–5.6	6.0–7.0	6, 29
Hematite	0.9–17.0	0.9–18.9	6–9, 10–17
Jarosite	2.1–5.3	2.4–7.1	6, 10, 11, 14, 18
Lepidocrocite	4.3–7.1	5.3–9.7	6, 7
Goethite	1.3–9.1	1.3–10.8	6, 7, 9–14
Ferrihydrite	3.9–13.8	5.2–14.6	6–8, 19
Ferroxyhyte	8.0–8.1	9.4–11.7	7
Limonite	6.8–14.5	7.5–14.6	14
Hematite + silica gel	1.1–33.2	1.2–33.5	20–21
Palagonitic material	1.3–10.2	1.4–10.6	6, 10, 13, 19, 22–28

n.a. = not available.
Sources of data: 1: Bell et al. (2000); 2: McSween et al. (1999); 3: Singer (1985); 4: Bell (1996); 5: Bell et al. (1990); 6: Morris et al. (2000); 7: Sherman et al. (1982); 8: Bishop et al. (2000); 9: Morris et al. (1985); 10: this study; 11: Grove et al. (1992); 12: Adams (1974); 13: Adams et al. (1986); 14: Hunt and Salisbury (1971); 15: Morris et al. (1983); 16: Taranik and Kruse (1989); 17: Wagner et al. (1987); 18: Clark et al. (1990); 19: Bishop and Pieters (1995); 20: Morris et al. (1989); 21: Morris and Lauer (1990); 22: Bell et al. (1993); 23: Bishop et al. (1998); 24: Buemi et al. (1998); 25: Bishop et al. (2001); 26: Farrand and Singer (1991); 27: Golden et al. (1993); 28: Morris et al. (2001); 29: Bishop and Murad (1996).

tions of the bands above ∼ 880 nm generally range between ∼ 0.95 and ∼ 1.1 for pure palagonitic materials and between ∼ 0.92 and 1.09 for Mars bright regions (Bell, 1996) and Pathfinder bright soils (Bell et al., 2000); exceptions occur for some iron oxides such as hematite (e.g., Bell et al., 1990). Consequently, mixtures of palagonitic material and mafic silicates approach a value of ∼ 1 with increasing palagonitic material content for reflectance ratios involving only longer wavelength ($\gtrsim$ 800 nm) bands. This is seen in Fig. 6 where the long wavelength reflectance ratios of the orthopyroxene + palagonitic material series approach a value of ∼ 1 with increasing palagonitic material abundance. The utility of the 1044/955 nm and 1003/931 nm band ratios for mafic silicate characterization are discussed in more detail below.

5.1.2. *Orthopyroxene compositional variations*

It is known that an increase in ferrous iron content, for a fixed grain size, results in an increase in the depth and width of Band I (e.g., Cloutis and Gaffey, 1991a). This relationship manifests itself in changes in a number of the reflectance ratios in the broad band data. The reflectance ratios which showed correlations with orthopyroxene ferrous iron content (Table 4) were the 860/955 and 1044/955 nm ratios for HST, and the 858/967, 1003/931, and 1003/967 nm ratios for Pathfinder. However other factors such as changes in grain size, degree of crystallinity, cation site occupancy variations, and the presence of additional cations will also affect this ratio. Thus, changes in these ratios are best applied to detecting relative changes in orthopyroxene ferrosilite (Fs, $FeSiO_3$) content but are less reliable for determining absolute Fs contents because of the confounding effects of grain size variations and the presence of additional mafic silicates. Variations in these reflectance ratios reliably attributable to Fs content variations account for ∼ 50% of the total variation in these reflectance ratios.

5.1.3. *Orthopyroxene grain size variations*

Variations in the grain size of mafic silicates are known to produce changes in overall reflectance and band depths, both of which will manifest themselves in broad band reflectance ratios. The depth of Band I increases with increasing grain size up to a size of approximately 150 μm, beyond which trends are less systematic, probably due to band saturation effects (Hunt and Salisbury, 1970; King et al., 1981; Cloutis, 1985; Crown and Pieters, 1987; Azuma and Fujii, 1989; Mustard et al., 1993b; Hiroi and Pieters, 1994). This increase in band depth with increasing grain size results in increases in the reflectance ratios that are sensitive to band depth, most prominently those involving the bands near the Band I center position (Table 4). In the HST data, increasing orthopyroxene grain size results in increases in the 1044/955, 740/955, and 740/1044 nm ratios and a decrease in the 860/1044 nm ratio. This is due to the fact that reflectance at 860 nm, being closer to the orthopyroxene band minimum, decreases at a greater rate than the reflectance at 1044 nm. Equivalent relationships exist for the Pathfinder band passes: increases in the 1003/931, 1003/967, 752/967, 752/1003, and 752/858 nm ratios, and a decrease in the 858/1003 nm ratio. Grain size variations generally account for between 80 and 100% of the total variation seen in these reflectance ratios (50% in the case of the 1003/931 and 1044/955 nm ratios). The combination of reflectance ratio changes associated with orthopyroxene grain size variations

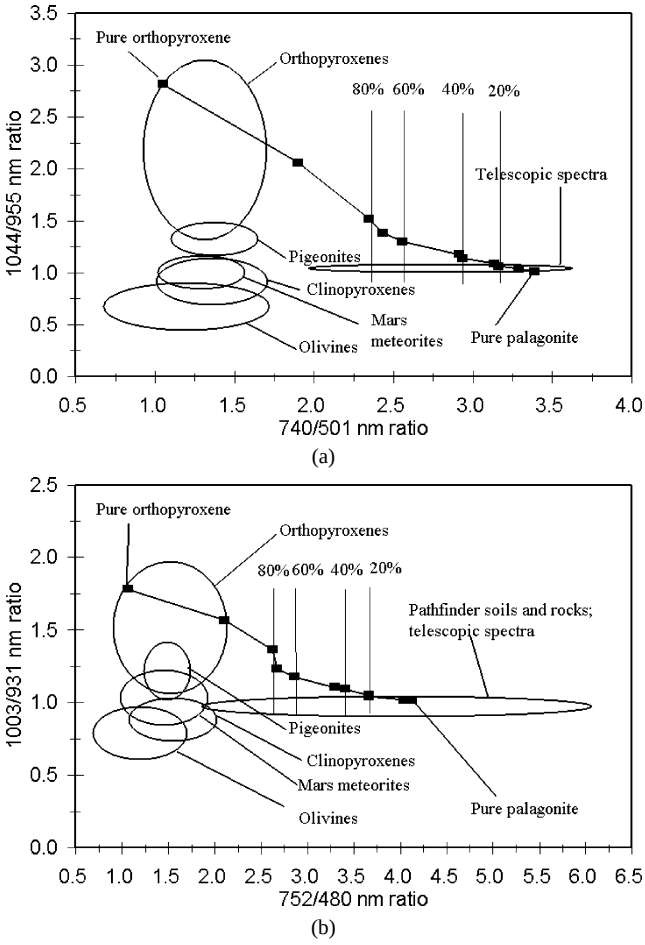

Fig. 6. 740/501 nm versus 1044/955 nm (a) and 752/480 nm versus 1003/931 nm (b) reflectance ratios of laboratory spectra of orthopyroxenes, pigeonites, clinopyroxenes, olivines, Mars meteorites, Mars telescopic and Pathfinder IMP rock and soil spectra, and orthopyroxene + palagonitic material intimate mixture spectra (points connected by line). The fields occupied by each of these groups are delineated by ellipses. The vertical lines indicate the values of the 740/501 nm (a) and 752/480 nm (b) ratios for 20, 40, 60 and 80 wt% palagonitic material in the main orthopyroxene + palagonitic material intimate mixture series. The pure palagonitic material and pure orthopyroxene are the rightmost and leftmost points, respectively in the series.

is unique (Table 4). Once again, because of the complications introduced by compositional and structural factors, relative changes in grain sizes are more tractable than absolute values.

5.1.4. Clinopyroxene grain size variations

Reflectance ratios for clinopyroxenes also exhibit a number of systematic variations as a function of grain size variations. With increasing grain size, the ratios involving wavelength bands in the 750–930 nm range versus the longest wavelength bands (1044 and 1003 nm) all generally increase with increasing grain size for a fixed composition up to approximately 150 μm grain size, beyond which the trends are less systematic, again probably due to band saturation effects in some cases (Table 4). This is expected from the fact that increasing grain size leads to increasing band depth (Azuma and Fujii, 1989; Mustard et al., 1993b; Lucey, 1998). The differences between orthopyroxene and clinopyroxene spectra in terms of the sign of the correlations (positive or negative) are related to the fact that the clinopyroxene Band I is located at longer wavelengths than the corresponding band in orthopyroxenes (Cloutis and Gaffey, 1991a, 1991b). Once again, the combination of reflectance ratio variations for this parameter is unique (Table 4). Clinopyroxene grain size variations can account for ∼ 80% of the total range exhibited by these reflectance ratios.

5.1.5. Clinopyroxene iron content variations

The wavelength position of Band I in clinopyroxenes has been found to decrease with increasing iron content in high-resolution spectra (Cloutis and Gaffey, 1991a). When deconvolved to the HST and Pathfinder band passes, increasing iron content results in a number of trends that are generally consistent between the equivalent HST and Pathfinder band passes (Table 4). These trends are in the directions expected from the relationship between iron content and absorption band position. Approximately 100% of the variation in the 1044/955 and 1003/967 nm and 50% of the variation in the other ratios for which trends were found (Table 4) can be attributed to clinopyroxene iron content variations. Once again, these trends are most reliable for determining relative changes in iron content as opposed to deriving absolute values because of the confounding effects of grain size variations and the presence of additional mafic silicates.

5.1.6. Pyroxene calcium content variations

Most martian meteorites contain abundant calcium-bearing pyroxenes such as pigeonite and augite (McSween and Treiman, 1998). Previous studies of pyroxene spectra determined that the wavelength position of Band I increases with increasing calcium content (Cloutis and Gaffey, 1991a). This relationship manifests itself in systematic variations in some of the reflectance ratios of the broad-band data. The various trends found (Table 4) are consistent with expectations, as the absorption band moves progressively toward longer wavelengths with increasing calcium content. The variation in reflectance ratios attributable to wollastonite (Wo, $CaSiO_3$) content variations is in the neighborhood of 50%. Once again, relative changes in the various reflectance ratios are more robust for determining relative changes in Wo content as opposed to deriving absolute values because of the confounding effects of other assemblage parameters.

5.1.7. Clinopyroxene abundance variations

The effects of increasing clinopyroxene abundance (in clinopyroxene + orthopyroxene mixtures) are quite similar to the trends found for olivine + orthopyroxene mixtures (see below) due to the fact that clinopyroxene and olivine are spectrally rather similar in the 400–1050 nm region: both are characterized by a broad absorption band in the 1050 nm region. With increasing clinopyroxene, the Band I absorption feature moves toward longer wavelengths, and this trend

is expressed in the relevant reflectance ratios. The various systematic trends that were found enable relative changes in clinopyroxene abundance to be discriminated from other variations in assemblage properties (Table 4). In addition, it was also found that the 673/740 (HST) and 671/752 nm reflectance ratios allow for discrimination of olivine (ratios generally > 1) versus clinopyroxene (ratios generally < 1) as pure end members. However, in the presence of palagonitic material or other mafic silicates, the two ratios tend to converge to values of < 1, reducing its utility for discriminating these two mafic silicates in palagonitic material-bearing mixtures.

5.1.8. Olivine grain size variations

Olivine is present in many martian meteorites and is the dominant phase in chassignites (McSween and Treiman, 1998; Folco et al., 1999). As was the case with pyroxenes, olivine shows a number of systematic changes in reflectance ratios involving the absorption feature in the 1050 nm region (Table 4). These trends are valid up to approximately 150-μm grain size, beyond which the trends are not systematic. Once again these systematic variations are related to the increase in the depth of the main absorption feature located near 1050 nm with increasing grain size (Hunt and Salisbury, 1970; Miyamoto et al., 1981; Cloutis, 1985; King and Ridley, 1987; Azuma and Fujii, 1989; Mustard et al., 1993b; Hiroi and Pieters, 1994; Mustard and Hays, 1997; Sunshine and Pieters, 1998).

5.1.9. Olivine iron content variations

The absorption feature of olivine located near 1050 nm moves to longer wavelengths and becomes broader with increasing iron content. This trend is expressed in expected trends in various reflectance ratios involving the bands nearest the major absorption feature located near 1050 nm (Table 4). The variations of the ratios for an increase in grain size of a single olivine from < 45 to 45–90 μm are greater than the same variations across the olivine compositional space. In addition, the 740/501 nm (HST) and 752/480 nm (Pathfinder) reflectance ratios increase with increasing iron content. This is probably due to the increase in absorption in the 300–500 nm region that accompanies increasing iron content.

5.1.10. Olivine abundance variations

Both orthopyroxene + olivine and clinopyroxene + olivine mixtures were available for this study. Olivine, clinopyroxene, and orthopyroxene exhibit enough spectral differences to allow for detection of increases in olivine abundances in mixtures with one or both of types of pyroxenes. Generally, less systematic trends were found for olivine + clinopyroxene mixtures versus olivine + orthopyroxene, probably because clinopyroxenes are more spectrally heterogeneous and similar to olivines than are orthopyroxenes (Table 4). Once again the various systematic trends that were found allow for relative changes in olivine abundance to be discriminated from other variations in assemblage properties.

5.2. Systematic spectral variations

Systematic variations were found for all of the parameters of interest (compositional changes, end member abundances, and grain size variations), as discussed above. In order to reduce ambiguities and uncertainties in interpretation, robust analysis should include all of the relevant band ratios presented in Table 4. This is because most reflectance ratios show variations as a function of changes in end member compositions, abundances, and grain sizes, but not all of the variations are systematic.

Given the large number of factors which can influence reflectance ratios and the limited number of useful reflectance ratios and band depth measurements which can be generated from broad band data, deriving absolute quantities for all mafic silicate ± palagonitic material mixture parameters is not robust. Consequently, the greatest utility of the various trends described above is to determine relative changes in assemblage parameters as opposed to deriving absolute values. Figure 7 shows the relationship between the pairs of reflectance ratios that permit the greatest discrimination of mafic silicates as well as expected trends (shown by arrows) with changes in mafic silicate parameters such as end member abundances, grain sizes and compositions. While the fields for most of the pure end members are largely separable, mineral mixtures (not shown) and the presence of palagonitic material (which causes the band ratios to approach a value of ~ 1) complicate the analysis. Note that many of these changes are similar in terms of how they affect these band ratios, and, as mentioned, in order to reconcile ambiguities, the full range of available band ratios (Table 4) should be utilized. As an example, the 1044/955 nm ratio increases as a function of multiple assemblage properties. Additional reflectance ratios are required to determine which of these parameters may be the likeliest cause of this variation.

Extending these results to deriving quantitative or semi-quantitative mineralogical information requires that multiple spectral parameters be considered simultaneously and/or that certain simplifying assumptions be made. As discussed previously increasing palagonitic material content affects all of the spectral ratios, including those involving the bands beyond ~ 700 nm which are most useful for mafic silicate mineralogical determinations. In order to derive quantitative mineralogical information, the 740/501 nm (for HST) and 752/480 nm (for Pathfinder) ratios (which are most effective for deriving palagonitic material abundances) must be coupled to the analysis so that the effects of changing palagonitic material abundance can be separated from changes in mafic silicate mineralogy. The data presented here are only strictly valid for the spectra included in this study since, as noted, palagonitic materials are highly variable both compositionally and spectrally.

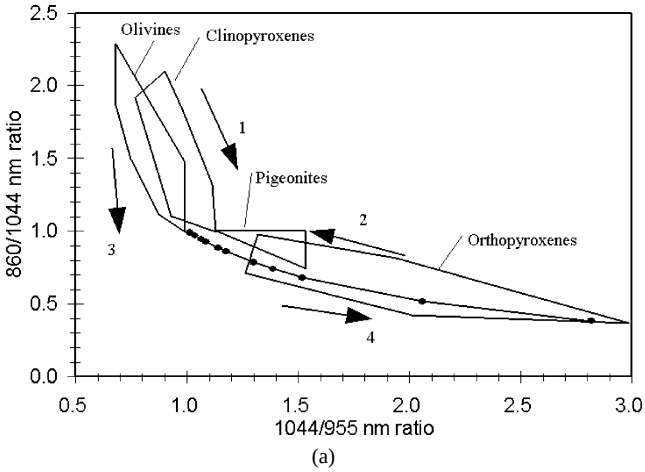

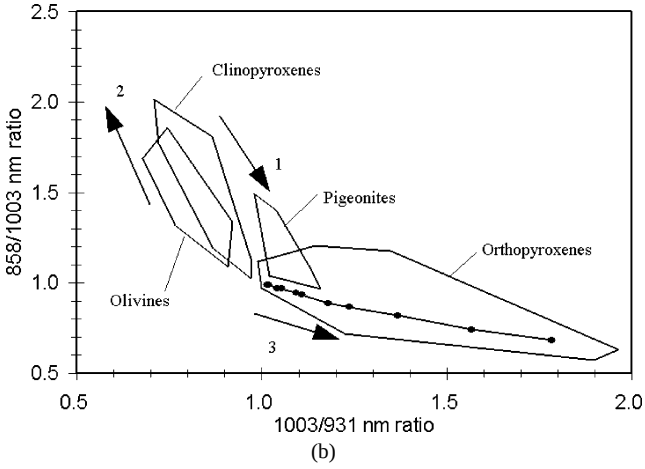

Fig. 7. (a) 1044/955 nm versus 860/1044 nm reflectance ratios of orthopyroxenes, clinopyroxenes, pigeonites, and olivines, and orthopyroxene + palagonitic material intimate mixture series (points connected by lines). Arrows indicate trends in reflectance ratios that are tabulated in Table 4: arrow 1: increasing clinopyroxene Fs content; arrow 2: increasing pyroxene Wo content, olivine grain size, olivine content (with orthopyroxene), clinopyroxene content (with orthopyroxene); arrow 3: increasing clinopyroxene grain size, olivine content (with orthopyroxene); arrow 4: increasing orthopyroxene Fs content, orthopyroxene grain size, olivine Fa content. (b) Same as (a) for the 1003/931 nm versus 858/1003 reflectance ratios. Arrow 1: increasing clinopyroxene Fs content, olivine Fa content, olivine content (with clinopyroxene); arrow 2: increasing clinopyroxene grain size, pyroxene Wo content, olivine grain size, olivine content (with orthopyroxene), clinopyroxene content (with orthopyroxene); arrow 3: increasing orthopyroxene grain size.

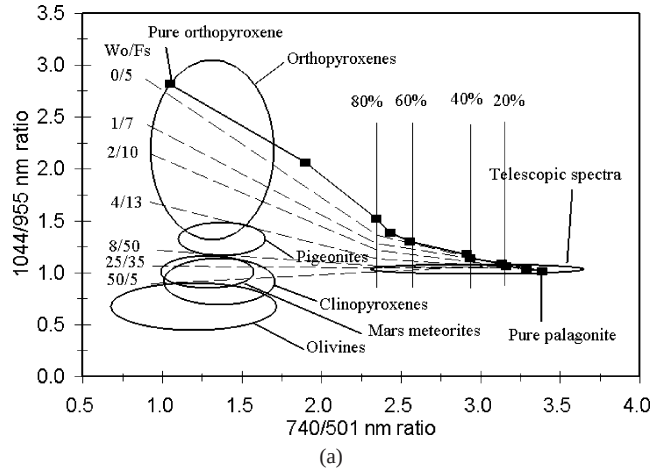

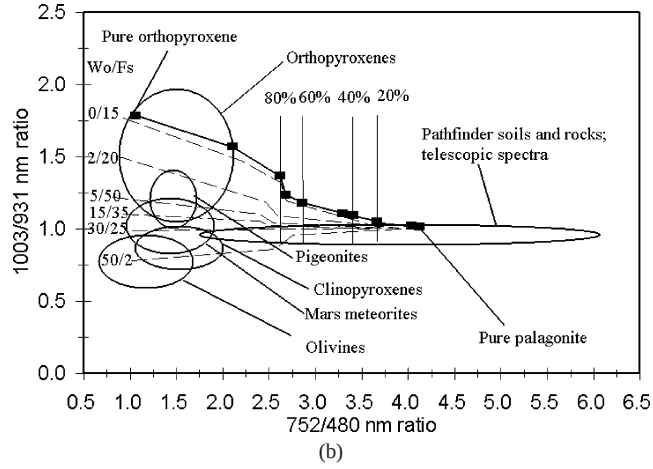

Fig. 8. Same as Fig. 6, with the addition of dashed lines indicating the expected trends for orthopyroxene or clinopyroxene + palagonitic material series. The intersection of the vertical lines (showing palagonitic material abundance) with the dashed lines can be used to constrain both palagonitic material abundance and pyroxene composition. The Wo abundances apply to the orthopyroxenes, pigeonites, and clinopyroxenes, while the top four dashed lines in (a) and top three dashed lines in (b) are for orthopyroxene Fs compositions, and the bottom three dashed lines in (a) and (b) are for clinopyroxene Fs compositions. A point plotting in this field can be used to constrain palagonitic material abundance and pyroxene composition, assuming a pyroxene + palagonitic material assemblage. See text for details on its application and constraints.

Dark region spectra and less bright soils (presumed to contain some contributions from mafic silicates) have 752/480 nm ratios as low as 1.8, suggestive of up to ~ 90% mafic silicates (Fig. 6). This is based on the assumption that the intimate mixtures of pyroxene + palagonitic material are spectrally representative of Mars fines + mafic silicates. As discussed previously, intimate mixtures are reasonable analogs of dust coatings in terms of how they affect mafic silicate absorption band wavelength positions, and they also simulate the reductions in mafic silicate band depths that accompany increasing thicknesses of coatings. Martian meteorite spectra have 740/501 reflectance ratios of between 1.0 and 1.7, well within the pure mafic silicates field (Fig. 6).

The 1044/955 nm ratio shows correlations with the Fe^{2+} and Wo contents of both orthopyroxene and clinopyroxene (Table 4), consequently Wo and Fs contours can be constructed in the 1044/955 versus 740/501 nm reflectance ratios field of Fig. 6a (Fig. 8a). The main orthopyroxene + palagonitic material series used in this study involving 45–90 μm sized orthopyroxene (Fs 13; Table 1) is also shown. The dashed lines are the expected reflectance ratio trends for mixtures of pyroxene + palagonitic material involving 45- to 90-μm sized mafic silicates. Note that the pure orthopyroxene point for this suggests that its Fs content is < 5. This is attributable to the scatter in the data relating the 1044/955

ratio to Fs content and the variations in this ratio attributed to grain size variations (and other factors for more complex assemblages) (Table 4); the data in Fig. 8 are generally accurate to within ± 5% Fs with the assumption of 45- to 90-μm sized pyroxene. This example serves to illustrate some of the ambiguities which can arise from incomplete interpretation of broad band spectral data. Similar relationships have been established for the Pathfinder IMP band passes (Fig. 8b). The limited data for mixtures involving < 45-μm sized mafic silicates (Table 2) suggests that for fine-grained mafic silicates mafic silicate abundances would be underestimated by about 20% using the trends presented in Fig. 8. This is probably due to the fact that finer-grained mafic silicates have a greater surface area than a comparable abundance of coarse-grained samples, resulting in a thinner average coating of the grains by palagonitic material.

One source of ambiguity that was found involves olivine versus clinopyroxene. The wavelength positions of the major absorption features in the 1000 nm region can overlap and the various reflectance ratios (Table 4) do not provide a robust unambiguous method for discriminating them in all cases. However, the major difference between these two minerals is the fact that olivine Band I consists of three partially overlapping absorption bands (Burns, 1970), and the shortest wavelength band affects both the 860 and 955 nm bands of the HST band set and 858, 931, and 967 bands of the IMP band set. Band depths at 860 and 955 nm were calculated as the difference between reflectance at 860 or 955 nm and a straight line continuum connecting the nearest available data points on either side of this value (Clark and Roush, 1984). Band depths at 858 and 931 nm were calculated in the same way but using reflectance values at 752 and 931 nm (for 858 nm band depths) and reflectance values at 858 and 1003 nm (for 931 nm band depths). When the two sets of band depths are compared, olivine and clinopyroxene become largely separable (Fig. 9; see also Fig. 5 for examples of the resampled spectra). Palagonitic material has band depths of ∼ 1. Thus with increasing palagonitic material abundance, values will converge toward the origin, possibly leading to ambiguities in distinguishing clinopyroxene from olivine. However, this method appears to be the best available method for distinguishing these two minerals with the available broad-band data band passes.

While the fields for the pure mafic silicate end members are largely separable using the various available spectral criteria, mixtures of the various mafic silicates (e.g., orthopyroxene + clinopyroxene) can fall within the pure mineral fields or between them, depending on both the composition of the mafic silicates and their abundances. In the latter case, a number of data points which fall in the region between the orthopyroxene and clinopyroxene fields of Fig. 7 (the area which would be connected by straight lines joining these two fields) would be readily recognized as two-pyroxene mixtures rather than single pyroxenes. In the former case, where two-pyroxene mixtures fall within the orthopyroxene or clinopyroxene fields of Fig. 7, they cannot be uniquely recognized using the data in Fig. 7 alone.

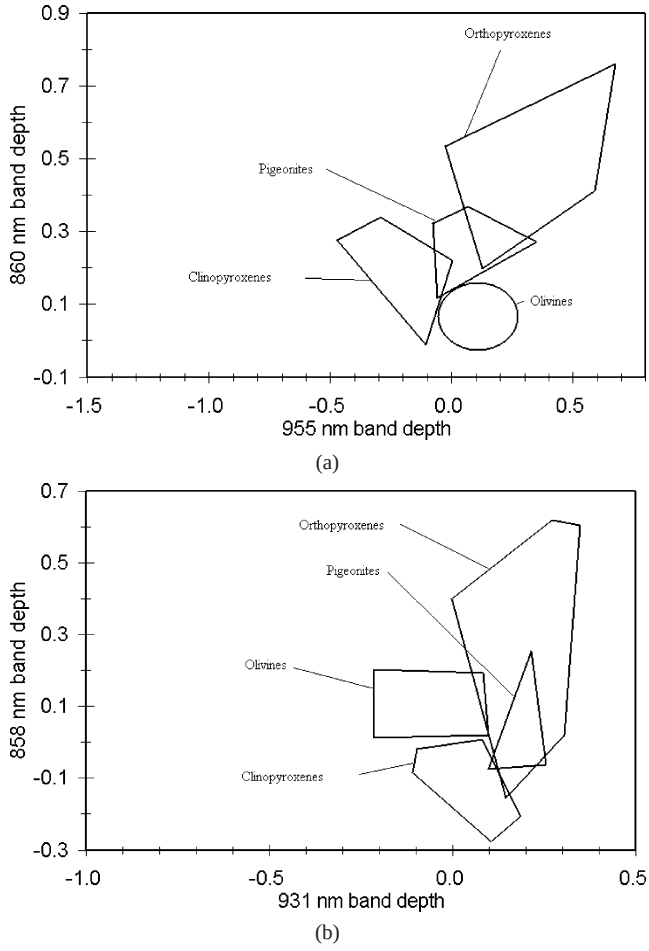

Fig. 9. 955 nm versus 860 nm (a) and 931 nm versus 858 nm (b) band depths for various mafic silicates. See text for description of band depth calculations.

However, constraints can be placed on the composition of a possible two-pyroxene mixture. The 1044/955 nm (HST) and 1003/931 nm (Pathfinder) reflectance ratios, that provide good discrimination between pure orthopyroxene and clinopyroxene, can be used to place such constraints. The trends expected for clinopyroxene + orthopyroxene mixtures as a function of Fs content are shown for both the HST (Fig. 10a) and Pathfinder (Fig. 10b) band passes. In the case of the HST band passes, since the 1044/955 nm ratio increases with decreasing clinopyroxene Fs content and increasing orthopyroxene Fs content, the trend lines cross each other at various points in the region. As an example of how this relationship can be used to constrain the properties of a two-pyroxene mixture consider an unknown spectrum with a 1044/955 nm reflectance ratio of 2 (Fig. 10a). Such a value constrains the orthopyroxene content of a two-pyroxene mixture to at least ∼ 60 wt% (where the horizontal line constructed at a 1044/955 nm ratio of 2 intersects the Fs 5 line), and less than ∼ Fs 15 (where the same horizontal line intersects the vertical axis at 100% orthopyroxene).

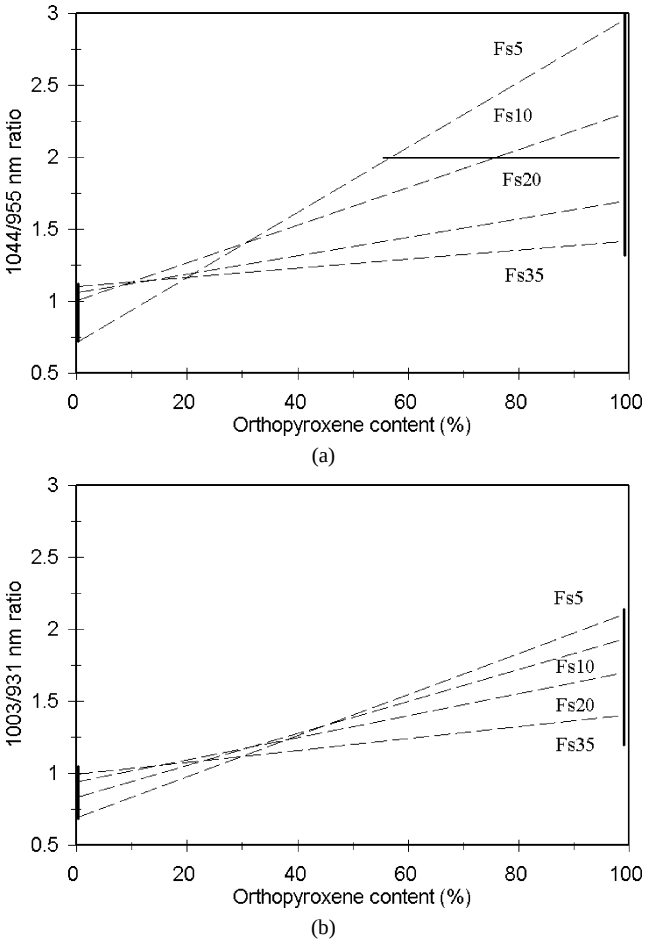

Fig. 10. 1044/955 nm (a) and 1003/931 nm (b) reflectance ratios for orthopyroxene + clinopyroxene mixtures versus orthopyroxene content. The dashed lines are the reflectance ratio trends for two-pyroxene equilibrium assemblages (for a given orthopyroxene Fs content).

A reflectance ratio of 2 can be accommodated by increasing orthopyroxene content accompanied by a decrease in Fs content because an inverse relationship exists between orthopyroxene Fs content and orthopyroxene abundance for a given 1044/955 nm value. A similar relationship exists for the Pathfinder band passes (Fig. 10b).

As noted earlier, the most robust application of the derived spectral trends is for ascertaining probable variations in end member properties (abundances, compositions, and grain size variations) in a relative sense; e.g., determining whether one area is more orthopyroxene-rich than another area. Reflectance ratios have been successfully employed in the past for examining spectral (and geological) variability on a hemispheric/global basis on Mars (e.g., Pinet and Chevrel, 1990), while differences in spectral properties have been used to infer geological variability on Mars (McSween et al., 1999; Bell et al., 2000). The rest of this discussion focuses on the use of multiple band ratios for deriving relative changes in target properties.

Of the mafic silicate parameters, end member abundances may be the most tractable parameter due to the fact that the end member group spectra are sufficiently different to allow changes in relative end member abundances to be ascertained. If a four-component mixture of orthopyroxene, clinopyroxene, olivine, and palagonitic material is assumed, the effects of changes in the relative abundances of the four phases are largely separable (Table 4). However the spectral variability of the end members and the limited number of useful band ratios precludes the use of such ratios for rigorous quantitative characterization of either end member abundances or absolute changes in end member abundances for such four-component mixtures.

Increasing grain sizes result in changes in spectral parameters that are different from those associated with end member abundance variations when multiple reflectance ratios are considered together (Table 4). The signs of these variations (positive or negative) are different for each mineral because of the unique spectral properties of each mineral class. Mafic silicate compositional variations are the most difficult parameter to derive due to the fact that the associated spectral changes are of lower magnitude than for grain size and end member abundance variations. As mentioned, inferred mineralogical variations are strengthened through the application of multiple reflectance ratio trends. The large number of non-systematic trends that were found (Table 4) add a level of complexity and uncertainty to the analysis, since these can affect the interpretation. While many parameters do not show trends when the full suite of samples is considered, smaller subsets of samples may exhibit trends. Therefore the data presented in Figs. 6, 7, and 8 and Table 4 should be used with caution and with an awareness that unique mineralogical interpretations may not be possible in all cases.

One of the major assumptions inherent in this analysis is that terrestrial palagonitic material is optically similar to the martian surface fines. Bell et al. (2000) and Morris et al. (2000) have shown that the spectral properties of martian surface fines, at least at the Pathfinder site, exhibit some diversity. From the perspective of deriving mafic silicate compositions from analysis of absorption features in the 1000 nm region, a number of ferric iron-bearing materials, such as hematite, maghemite, akagenite, schwertmannite, jarosite, lepidocrocite, goethite, and ferrihydrite exhibit an absorption feature in the 800–950 nm region that could superficially be confused with pyroxene. However as Bell et al. (2000) noted, if this feature is attributed to these ferric iron-bearing phases, an increase in the abundance of this material should also be accompanied by increasing absorption shortward of ~ 700 nm. With the exception of a few of the hematite and goethite samples, the spectra of these phases exhibit 740/501 and 752/480 nm reflectance ratios of > 2. By contrast, pure mafic silicates and martian meteorites have 740/501 or 752/480 nm reflectance ratio of < 2 (Fig. 11). As a result, increasing band depths in the 900–1000 nm region due to increasing pyroxene abundance will be accompanied by a decrease in the 740/501 nm or 752/480 nm ratios, whereas increasing ferric iron-bearing

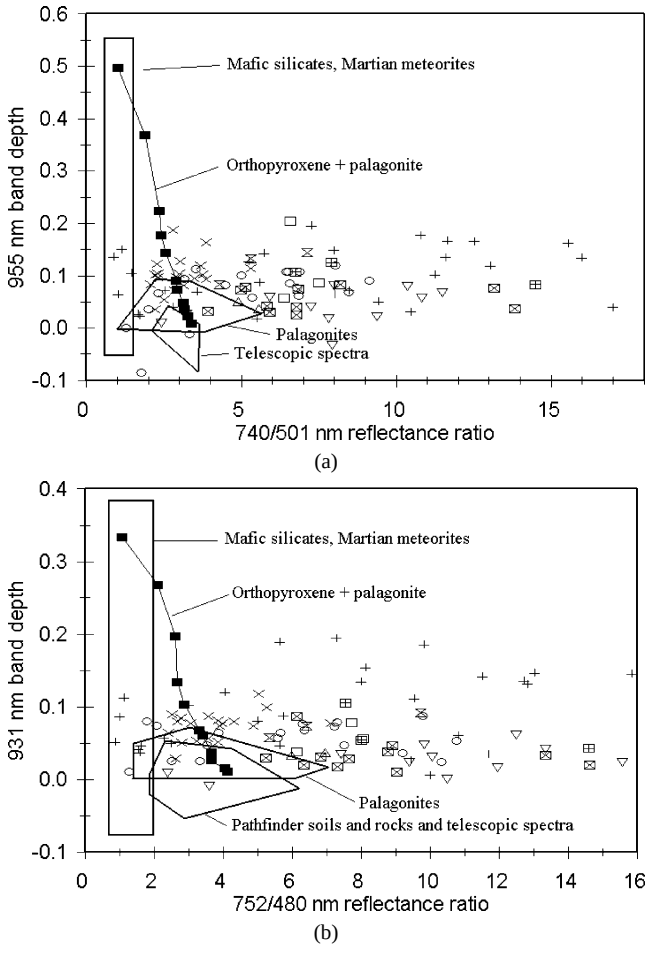

Fig. 11. 955 nm band depth versus 740/501 nm reflectance ratio (a) and 931 nm band depth versus 752/480 nm reflectance ratio (b) for the various spectra used in this study. ■—orthopyroxene + palagonitic material intimate mixture series; □—akagenite; ▽—maghemite; △—schwertmannite; +—hematite; ×—jarosite; ⧖—lepidocrocite; ○—goethite; ⊠—ferrihydrite; |—ferroxyhyte; ⊞—limonite. The regions occupied by mafic silicates (orthopyroxenes, pigeonites, clinopyroxenes, olivines) and martian meteorites, and Pathfinder IMP soil and rock spectra and telescopic spectra are delineated by polygons. The main orthopyroxene + palagonitic material intimate mixture series is represented by the solid squares connected by the solid line.

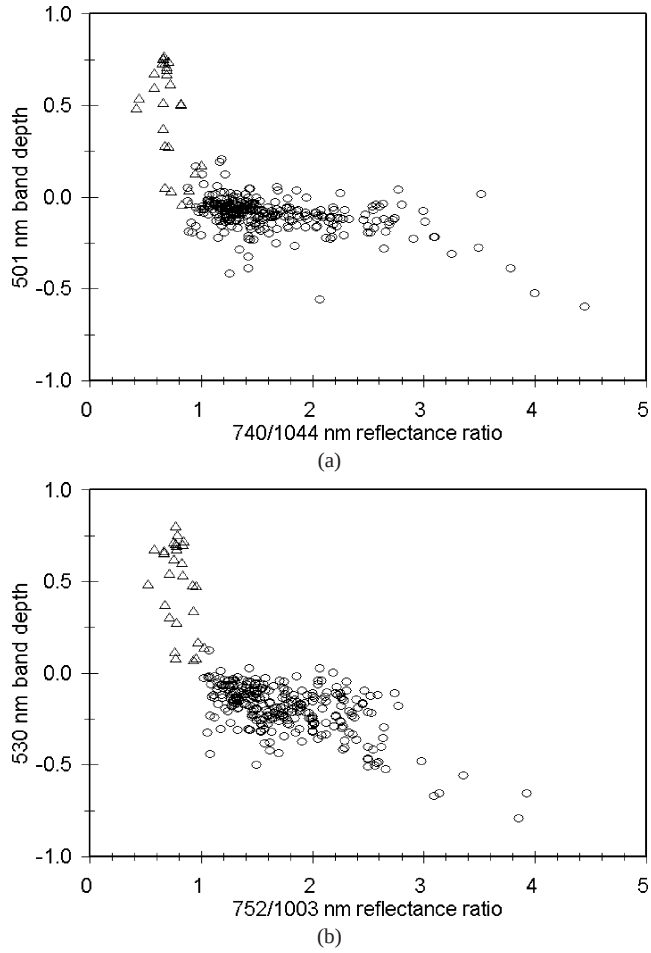

Fig. 12. 501 nm band depth versus 740/1044 nm (a) and 530 nm band depth versus 752/1003 nm (b) reflectance ratios for hematite (△), and mafic silicates and martian meteorites (○).

phase abundance will generally be accompanied by an increase in these ratios. Such a relationship was also found by Bell et al. (2000) from analysis of Pathfinder IMP spectra.

These results are consistent with the interpretation of Bell et al. (2000) for Pathfinder soils presumed to contain crystalline ferric oxides. Hematite appears to be the most difficult ferric iron-bearing phase to distinguish from mafic silicates using reflectance ratios beyond ∼ 750 nm because its overall spectral shape in this region is most similar to pyroxenes (e.g., McSween et al., 1999; Bell et al., 2000). The most reliable spectral discriminators which were found involve the depth of the "bands" at 530 nm (IMP) and 501 nm (HST) and reflectance ratios of the longer wavelength bands (Fig. 12). All of the hematite samples, including those which overlap the mafic silicate fields of Fig. 11, have larger 530 nm band depths than the mafic silicates; most of the hematite samples have larger 501 nm band depths than the mafic silicates. In the case of the longer wavelength bands, reflectance ratios involving the longest wavelength band with the next shortest bands (e.g., 1003/967 nm and 1003/931 nm for HST, and 1044/955 for Pathfinder) have ratios of generally > 1 for the mafic silicates versus generally < 1 for hematite, providing a second reliable spectral discriminator.

The various reflectance ratios that are described above for discriminating crystalline ferric oxide minerals from mafic silicates complement those of other investigators. As an example, Bishop et al. (1998b) used Pathfinder reflectance ratios in the 600 nm region to discriminate ferrihydrite- from schwertmannite-bearing soils. Morris et al. (2000) advocates the use of the peak band (at either 752 or 801 nm) as an additional indicator of ferric mineralogy.

6. Summary and conclusions

The simplified geology of large regions of Mars seems to consist of mafic silicates (primarily pyroxenes) and a fine-

grained, windblown dust component. Palagonitic material has been found to be a reasonable spectral analogue for this dust component at wavelengths below ~ 1200 nm. The inferred widespread presence of mafic silicates on Mars is strengthened by the fact that mafic silicates are the petrologically and spectrally dominant component of martian meteorites. Laboratory spectra of pyroxene + palagonitic material mixtures show that palagonitic material has little effect on the wavelength position of pyroxene absorption bands in the 1000 nm region, and allows pyroxene composition to be determined even in the presence of 90% linear or intimate mixtures of palagonitic material.

When remote sensing measurements of Mars are obtained using broad band passes typical of past or planned future multispectral imaging systems, the uniqueness of mineralogical information that can be derived decreases. Simplifying assumptions are required to enable absolute assemblage properties such as mafic silicate compositions, abundances, and grain sizes to be derived. However the use of multiple reflectance ratio trends still allows relative changes in mineralogy, particularly mafic silicate end member abundances, to be determined. This is due to the fact that while some trends are common to more than one mineralogical parameter, the full suite of trends is generally unique to a particular assemblage parameter (e.g., end-member compositions, end-member abundances, grain sizes). In general, reflectance ratios involving the lowest wavelength band passes ($\lesssim 750$ nm) are most useful for assessing the presence and relative abundance of palagonitic material-like ferric alteration products, while longer wavelength band passes ($\gtrsim 750$ nm) are most useful for characterizing mafic silicates. Our results indicate that ferric iron-bearing materials can be discriminated from mafic silicates based on the differences in spectral slope below about 750 nm and absorption features in the 500–550 nm region. These differences can be used in conjunction with other reflectance ratios to provide discrimination of these two groups of materials.

Spectral analysis using broad band data is most robust when these various trends are used together to ascertain relative changes in assemblage parameters as opposed to absolute variations. These results could also help optimize the selection of wavelengths and band widths on future Mars VIS-NIR multispectral remote sensing instruments.

Acknowledgments

We thank Dr. Ted Roush at the NASA Ames Research Center and Dr. Dick Morris at the NASA Johnson Space Center, and the staff at the Smithsonian Institution National Museum of Natural History for providing the palagonitic materials and some of the mineral samples used in this study. We also thank Dr. Takahiro Hiroi and Dr. Carlé Pieters for providing generous access to the NASA-supported RELAB spectrometer facility for the spectral measurements. X-ray diffraction data were acquired and analyzed through the generous support and assistance of Dr. Frank Hawthorne and Mr. Neil Ball of the Department of Geological Sciences at the University of Manitoba. The authors also thank Mr. Trevor Mueller for his assistance with the spectral data analysis. This study was supported by a start-up and discretionary grant from the University of Winnipeg, and research grants from Sigma Xi and the Geological Society of America to EAC, and by a grant from the NASA Planetary Geology and Geophysics Program (NAG5-10636) to JFB. Sincere thanks to Janice Bishop and Scott Murchie for their thorough reviews and thoughtful comments on a sometimes dense manuscript and for pointing out some apparent shortcomings.

References

Adams, J.B., 1974. Visible and near-infrared diffuse reflectance spectra of pyroxenes as applied to remote sensing of solid objects in the Solar System. J. Geophys. Res. 79, 4829–4836.

Adams, J.B., 1975. Interpretation of visible and near-infrared diffuse reflectance spectra of pyroxenes and other rock-forming minerals. In: Karr Jr., C. (Ed.), Infrared and Raman Spectroscopy of Terrestrial Minerals. Academic Press, New York, pp. 91–116.

Adams, J.B., Hörz, F., Gibbons, R.V., 1979. Effects of shock-loading on the reflectance spectra of plagioclase, pyroxene, and glass. In: Proc. Lunar Planet. Sci. Conf. 10th, pp. 1–3. Abstract.

Adams, J.B., Smith, M.O., Johnson, P.E., 1986. Spectral mixture modeling: a new analysis of rock and soil types at the Viking 1 Lander site. J. Geophys. Res. 91, 8098–8112.

Allen, C.C., Morris, R.V., Lauer Jr., H.V., McKay, D.S., 1993. Effects of microscopic iron metal on the reflectance spectra of glass and minerals. In: Proc. Lunar Planet. Sci. Conf. 24th, pp. 17–18. Abstract.

Azuma, H., Fujii, N., 1989. Grain size effects on spectral reflectance of Ol, Opx and Cpx minerals applied to the Hull quotient method. In: Proc. Lunar Planet. Sci. Conf. 20th, pp. 32–33. Abstract.

Bandfield, J.L., Hamilton, V.E., Christensen, P.R., 2000. A global view of martian surface composition from MGS-TES. Science 287, 1626–1630.

Banin, A., Han, F.X., Kan, I., Cicelsky, A., 1997. Acidic volatiles and the Mars soil. J. Geophys. Res. 102, 13341–13356.

Bartels, K.S., Burns, R.G., 1989. Oxidized olivines on Mars: spectroscopic investigations of heat-induced aerial oxidation products. In: Proc. Lunar Planet. Sci. Conf. 20th, pp. 44–45. Abstract.

Basaltic Volcanism Study Project, 1981. Basaltic Volcanism on the Terrestrial Planets. Pergamon, New York.

Bell III, J.F., 1996. Iron, sulfate, carbonate, and hydrated minerals on Mars. In: Dyar, M.D., McCammon, C., Schaefer, M.W. (Eds.), Mineral Spectroscopy: A Tribute to Roger G. Burns. Geochemical Society, New York, pp. 359–380.

Bell III, J.F., McCord, T.B., Owensby, P.D., 1990. Observational evidence of crystalline iron oxides on Mars. J. Geophys. Res. 95, 14447–14461.

Bell III, J.F., Morris, R.V., Adams, J.B., 1993. Thermally altered palagonitic tephra: a spectral and process analog to the soil and dust of Mars. J. Geophys. Res. 98, 3373–3385.

Bell III, J.F., Klassen, D.R., Moersch, J.E., Golisch, W.F., Griep, D.M., Kaminski, C.D., Martin, P., Dumas, C., Clark, R.N., Cloutis, E.A., 1997. High spatial resolution near-IR imaging spectroscopy of Mars from the IRTF during 1996–97. Bull. Am. Astron. Soc. 29, 963.

Bell III, J.F., McSween Jr., H.Y., Crisp, J.A., Morris, R.V., Murchie, S.L., Bridges, N.T., Johnson, J.R., Britt, D.T., Golombek, M.P., Moore, H.J., Ghosh, A., Bishop, J.L., Anderson, R.C., Brückner, J., Economou, T., Greenwood, J.P., Gunnlaugsson, H.P., Hargraves, R.M., Hviid, S., Knudsen, J.M., Madsen, M.B., Reid, R., Rieder, R., Soderblom, L.,

2000. Mineralogical and compositional properties of martian soil and dust: results from Mars Pathfinder. J. Geophys. Res. 105, 1721–1755.

Bell III, J.F., Squyres, S.W., Herkenhoff, K.E., Maki, J.N., Arneson, H.M., Brown, D., Collins, S.A., Dingizian, A., Elliot, S.T., Hagerott, E.C., Hayes, A.G., Johnson, M.J., Johnson, J.R., Joseph, J., Kinch, K., Lemmon, M.T., Morris, R.V., Scherr, L., Schwochert, M., Shepard, M.K., Smith, G.H., Sohl-Dickstein, J.N., Sullivan, R., Sullivan, W.T., Wadsworth, M., 2003. The Mars Exploration Rover Athena Panoramic Camera (Pancam) investigation. J. Geophys. Res. In press.

Berkley, J.L., Keil, K., Prinz, M., 1980. Comparative petrology and origin of Governador Valadares and other nakhlites. In: Proc. Lunar Planet. Sci. Conf. 11th, pp. 1089–1102.

Besancon, J.R., Burns, R.G., Pratt, S.F., 1991. Reflectance spectra of Fe^{2+}–Mg^{2+} disordered pyroxenes: implications to remote-sensed spectra of planetary surfaces. In: Proc. Lunar Planet. Sci. Conf. 22nd, pp. 95–96. Abstract.

Bishop, J.L., Murad, E., 1996. Schwertmannite on Mars? Spectroscopic analysis of schwertmannite, its relationship to other ferric minerals, and its possible presence in the surface material on Mars. In: Dyar, M.D., McCammon, C., Schaeffer, M.W. (Eds.), Mineral Spectroscopy: A Tribute to Roger G. Burns. Geochemical Society, New York, pp. 337–358.

Bishop, J.L., Pieters, C.M., 1995. Low-temperature and low atmospheric pressure infrared reflectance spectroscopy of Mars soil analog materials. J. Geophys. Res. 100, 5369–5379.

Bishop, J.L., Pieters, C.M., Hiroi, T., Mustard, J.F., 1998a. Spectroscopic analysis of martian meteorite Allan Hills 84001 powder and applications for spectral identification of mineral and other soil components on Mars. Meteorit. Planet. Sci. 33, 699–707.

Bishop, J.L., Scheinost, A., Bell III, J.F., Britt, D., Johnson, J.R., Murchie, S., 1998b. Ferrihydrite–schwertmannite–silicate mixtures as a model of martian soils measured by Pathfinder. In: Proc. Lunar Planet. Sci. Conf. 29th. Abstract #1803 [CD-ROM].

Bishop, J.L., Mancinelli, R.L., Olsen, M., Wagner, P.A., Zent, A.P., 2000. Ferrihydrite alteration to magnetite, maghemite and hematite: implications for iron oxides on Mars. In: Proc. Lunar Planet. Sci. Conf. 31st. Abstract #1946 [CD-ROM].

Bishop, J.L., Schiffman, P., Murad, E., Southard, R., 2001. Iceland as a model for chemical alteration on Mars. In: Proc. Lunar Planet. Sci. Conf. 32nd. Abstract #1435 [CD-ROM].

Boctor, N.Z., Meyer, H.O.A., Kullerud, G., 1976. Lafayette meteorite: petrology and opaque mineralogy. Earth Planet. Sci. Lett. 32, 69–76.

Bruckenthal, E.A., 1987. The dehydration of phyllosilicates and palagonites: reflectance spectroscopy and differential scanning calorimetry. MSc thesis. Univ. Hawaii, Honolulu.

Buemi, A., Cimino, G., Strazzulla, G., 1998. Characterization of Etnean soils and application to Mars. J. Geophys. Res. 103, 13667–13674.

Burns, R.G., 1970. Crystal field spectra and evidence of cation ordering in olivine minerals. Am. Mineral. 55, 1608–1632.

Cattermole, P., 1990. Volcanic flow development at Alba Patera, Mars. Icarus 83, 453–493.

Christensen, P.R., Anderson, D.L., Chase, S.C., Clancy, R.T., Clark, R.N., Conrath, B.J., Kieffer, H.H., Kuzmin, R.O., Malin, M.C., Pearl, J.C., Roush, T.L., Smith, M.D., 1998. Results from the Mars Global Surveyor Thermal Emission Spectrometer. Science 279, 1692–1697.

Christensen, P.R., Bandfield, J.L., Smith, M.D., Hamilton, V.E., Clark, R.N., 2000. Identification of a basaltic component on the martian surface from Thermal Emission Spectrometer data. J. Geophys. Res. 105, 9609–9621.

Clancy, R.T., Lee, S.W., Gladstone, G.R., McMillan, W.W., Roush, T., 1995. A new model for Mars atmospheric dust based upon analysis of ultraviolet through infrared observations from Mariner 9, Viking, and Phobos. J. Geophys. Res. 100, 5251–5263.

Clark, R.N., Roush, T.L., 1984. Reflectance spectroscopy: quantitative analysis techniques for remote sensing applications. J. Geophys. Res. 89, 6329–6340.

Clark, R.N., King, T.V.V., Klejwa, M., Swayze, G.A., Vergo, N., 1990. High spectral resolution reflectance spectroscopy of minerals. J. Geophys. Res. 95, 12653–12680.

Cloutis, E.A., 1985. Interpretive techniques for reflectance spectra of mafic silicates. MSc thesis. Univ. Hawaii, Honolulu.

Cloutis, E.A., Bell III, J.F., 2000. Diaspores and related hydroxides: spectral–compositional properties and implications for Mars. J. Geophys. Res. 105, 7053–7070.

Cloutis, E.A., Gaffey, M.J., 1991a. Pyroxene spectroscopy revisited: spectral–compositional correlations and relationship to geothermometry. J. Geophys. Res. 96, 22809–22826.

Cloutis, E.A., Gaffey, M.J., 1991b. Spectral–compositional variations in the constituent minerals of mafic and ultramafic assemblages and remote sensing implications. Earth Moon Planets 53, 11–53.

Cloutis, E.A., Gaffey, M.J., Jackowski, T.L., Reed, K.L., 1986. Calibrations of phase abundance, composition, and particle size distribution for olivine–orthopyroxene mixtures from reflectance spectra. J. Geophys. Res. 91, 11641–11653.

Cooper, C.D., Mustard, J.F., 1999. Effects of very fine particle size on reflectance spectra of smectite and palagonitic soil. Icarus 142, 557–570.

Crown, D.A., Pieters, C.M., 1987. Spectral properties of plagioclase and pyroxene mixtures and the interpretation of lunar soil spectra. Icarus 72, 492–506.

Cruikshank, D.P., Tholen, D.J., Hartmann, W.K., Bell, J.F., Brown, R.H., 1991. Three basaltic Earth-approaching asteroids and the source of the basaltic meteorites. Icarus 89, 1–13.

Dodd, R.T., 1981. Meteorites: A Chemical-Petrologic Synthesis. Cambridge Univ. Press, New York.

Eckstrand, O.R. (Ed.), 1984. Canadian Mineral Deposit Types: A Geological Synopsis. Canadian Government Publishing Centre, Ottawa. Geol. Surv. Canada, Economic Geology Report 36.

Evans, A.M., 1980. An Introduction to Ore Geology. Blackwell, Oxford, UK.

Farrand, W.H., Singer, R.B., 1991. Spectral analysis and mapping of palagonite tuffs of Pavant Butte, Millard County, Utah. Geophys. Res. Lett. 18, 2237–2240.

Feierberg, M.A., Larson, H.P., Fink, U., Smith, H.A., 1980. Spectroscopic evidence for two achondrite parent bodies: Asteroids 349 Dembowska and 4 Vesta. Geochim. Cosmochim. Acta 44, 513–524.

Finnerty, A.A., Phillips, R.J., Banerdt, W.B., 1988. Igneous processes and closed system evolution of the Tharsis region of Mars. J. Geophys. Res. 93, 10225–10235.

Fischer, E.M., Pieters, C.M., 1993. The continuum slope of Mars: bidirectional reflectance investigations and applications to Olympus Mons. Icarus 102, 185–202.

Floran, R.J., Prinz, M., Hlava, P.F., Keil, K., Nehru, C.E., Hinthorne, J.R., 1978. The Chassigny meteorite: a cumulate dunite with hydrous amphibole-bearing melt inclusions. Geochim. Cosmochim. Acta 42, 1213–1229.

Folco, L., Franchi, I.A., Scherer, P., Schultz, L., Pillinger, C.T., 1999. Dar al Gani 489 basaltic shergottite: a new find from the Sahara likely paired with Dar al Gani 476. Meteorit. Planet. Sci. Suppl. 34, A36–A37.

Gaffey, M.J., 1974. A systematic study of the spectral reflectivity characteristics of the meteorite classes with applications to the interpretation of asteroid spectra for mineralogical and petrological information. PhD dissertation. MIT, Cambridge, MA.

Gaffey, M.J., 1976. Spectral reflectance characteristics of the meteorite classes. J. Geophys. Res. 81, 905–920.

Gaffey, M.J., McCord, T.B., 1979. Mineralogical and petrological characterizations of asteroid surface materials. In: Gehrels, T. (Ed.), Asteroids. Univ. of Arizona Press, Tucson, pp. 688–723.

Gaffey, M.J., Bell, J.F., Brown, R.H., Burbine, T.H., Piatek, J.L., Reed, K.L., Chaky, D.A., 1993a. Mineralogical variations within the S-type asteroid class. Icarus 106, 573–602.

Gaffey, M.J., Burbine, T.H., Binzel, R.P., 1993b. Asteroid spectroscopy: progress and perspectives. Meteoritics 28, 161–187.

Golden, D.C., Morris, R.V., Ming, D.W., Lauer Jr., H.V., Yang, S.R., 1993. Mineralogy of three slightly palagonitized basaltic tephra samples from the summit of Mauna Kea, Hawaii. J. Geophys. Res. 98, 3401–3411.

Greeley, R., Crown, D.A., 1990. Volcanic geology of Tyrrhena Patera, Mars. J. Geophys. Res. 95, 7133–7149.

Gregg, T.K.P., Williams, S.N., 1996. Explosive mafic volcanoes on Mars and Earth: deep magma sources and rapid rise rate. Icarus 122, 397–405.

Grove, C.I., Hook, S.J., Paylor II, E.D., 1992. Laboratory Reflectance Spectra of 160 Minerals, 0.4 to 2.5 micrometers. Jet Propulsion Laboratory Publ. 92-2. Jet Propulsion Laboratory, Pasadena, CA.

Hay, R.L., Iijima, A., 1968. Nature and origin of palagonite tuffs of the Honolulu Group on Oahu, Hawaii. Geol. Soc. Am. Mem. 116, 331–376.

Hazen, R.M., Bell, P.M., Mao, H.K., 1978. Effects of compositional variation on absorption spectra of lunar pyroxenes. In: Proc. Lunar Planet. Sci. Conf. 9th, pp. 2919–2934.

Hiroi, T., Takeda, H., 1989. A method of converting reflectance spectra into absorption coefficient spectra of mineral mixtures for application to asteroidal surface mineralogy. In: Proc. Lunar Planet. Sci. Conf. 20th, pp. 418–419. Abstract.

Hiroi, T., Miyamoto, M., Takano, Y., 1985. An assignment of photon absorptions to Fe^{2+} and Cr^{3+} in pyroxenes and olivine by crystal field theory. In: Proc. Lunar Planet. Sci. Conf. 16th, pp. 356–357. Abstract.

Hiroi, T., Pieters, C.M., 1994. Estimation of grain sizes and mixing ratios of fine powder mixtures of common geologic materials. J. Geophys. Res. 99, 10867–10879.

Huguenin, R.L., 1987. The silicate component of martian dust. Icarus 70, 162–188.

Hunt, G.R., Salisbury, J.W., 1970. Visible and near-infrared spectra of minerals and rocks. I. Silicate minerals. Mod. Geol. 1, 283–300.

Hunt, G.R., Salisbury, J.W., Lenhoff, C.J., 1971. Visible and near-infrared spectra of minerals and rocks. III. Oxides and hydroxides. Mod. Geol. 2, 195–205.

Hunt, G.R., Salisbury, J.W., Lenhoff, C.J., 1973. Visible and near-infrared spectra of minerals and rocks. VI. Additional silicates. Mod. Geol. 4, 85–106.

Johnson, J.R., Grundy, W.M., 2000. Two-layer modeling of visible/near-infrared reflectance spectra of basalts coated with JSC-1 palagonite soil. In: Proc. Lunar Planet. Sci. Conf. 31st. Abstract #1724 [CD-ROM].

Johnson, P.E., Smith, M.O., Adams, J.B., 1992. Simple algorithm for remote determination of mineral abundances and particle sizes from reflectance spectra. J. Geophys. Res. 97, 2649–2657.

Johnson, J.R., Kirk, R., Soderblom, L.A., Gaddis, L., Reid, R.J., Britt, D.T., Smith, P., Lemmon, M., Thomas, N., Bell III, J.F., Bridges, N.T., Anderson, R., Herkenhoff, K.E., Maki, J., Murchie, S., Dummel, A., Jaumann, R., Trauthan, F., Arnold, G., 1999. Preliminary results on photometric properties of materials at the Sagan Memorial Station, Mars. J. Geophys. Res. 104, 8809–8830.

King, T.V.V., Ridley, W.I., 1987. Relation of the spectroscopic reflectance of olivine to mineral chemistry and some remote sensing implications. J. Geophys. Res. 92, 11457–11469.

King, T.V.V., Pieters, C.M., Sandlin, D.L., 1981. Particulate mineral mixtures: the relation of albedo and apparent absorption band strength. In: Proc. Lunar Planet. Sci. Conf. 12th, pp. 547–549. Abstract.

Kinoshita, M., Miyamoto, M., 1990. A model for analysis of the spectral reflectance of mineral mixtures. Proc. NIPR Symp. Antarct. Meteorites 3, 230–239.

Lindsley, D.H., 1983. Pyroxene thermometry. Am. Mineral. 68, 477–493.

Lindsley, D.H., Andersen, D.J., 1983. A two-pyroxene thermometer. In: Proc. Lunar Planet. Sci. Conf. 13th, Part 2, J. Geophys. Res. Suppl. 88, A887–A906.

Lopes, R.M.C., Kilburn, C.R.J., 1990. Emplacement of lava flow fields: application of terrestrial studies to Alba Patera, Mars. J. Geophys. Res. 95, 14383–14497.

Lucey, P.G., 1998. Model near-infrared optical constants of olivine and pyroxene as a function of iron content. J. Geophys. Res. 103, 1703–1713.

Lundberg, L.L., Crozaz, G., McSween Jr., H.Y., 1990. Rare Earth elements in minerals of the ALHA77005 shergottite and implications for its parent magma and crystallization history. Geochim. Cosmochim. Acta 54, 2535–2547.

Mason, B., Nelen, J.A., Muir, P., Taylor, S.R., 1975. The composition of the Chassigny meteorite. Meteoritics 11, 21–27.

McCord, T.B., Clark, R.N., 1979. The Mercury soil: presence of Fe^{2+}. J. Geophys. Res. 84, 7664–7668.

McCord, T.B., Adams, J.B., Johnson, T.V., 1970. Asteroid Vesta: spectral reflectivity and compositional implications. Science 168, 1445–1447.

McFadden, L.A., 1987. Spectral reflectance of SNC meteorites: relationship to martian surface composition. In: MEVTV Workshop on Nature and Composition of Surface of Mars, LPI Tech. Rep. 88-05. Lunar and Planetary Institute, Houston, pp. 88–90. Abstract.

McSween Jr., H.Y., 1985. SNC meteorites: clues to martian petrologic evolution? Rev. Geophys. 23, 391–416.

McSween Jr., H.Y., Jarosewich, E., 1983. Petrogenesis of the Elephant Moraine A79001 meteorite: multiple magma pulses on the shergottite parent body. Geochim. Cosmochim. Acta 47, 1501–1513.

McSween Jr., H.Y., Murchie, S.L., 1999. Rocks at the Mars Pathfinder landing site. Am. Sci. 87, 36–45.

McSween Jr., H.Y., Treiman, A.H., 1998. Martian meteorites. In: Papike, J.J. (Ed.), Planetary Materials. Mineralogical Society of America, Washington, DC. Chapter 6.

McSween Jr., H.Y., Taylor, L.A., Stolper, E.M., 1979. Allan Hills 77005: a new meteorite type found in Antarctica. Science 204, 1201–1203.

McSween Jr., H.Y., Murchie, S.L., Crisp, J.A., Bridges, N.T., Anderson, R.C., Bell III, J.F., Britt, D.T., Brückner, J., Dreibus, G., Economou, T., Ghosh, A., Golombek, M.P., Greenwood, J.P., Johnson, J.R., Moore, H.J., Morris, R.V., Parker, T.J., Rieder, R., Singer, R., Wänke, H., 1999. Chemical, multispectral, and textural constraints on the composition and origin of rocks at the Mars Pathfinder landing site. J. Geophys. Res. 104, 8679–8715.

Mikouchi, T., Miyamoto, M., McKay, G.A., 1998. Mineralogy of Antarctic basaltic shergottite Queen Alexandra Range 94201: similarities to Elephant Moraine A79001 (lithology B) martian meteorite. Meteorit. Planet. Sci. 33, 181–189.

Miyamoto, M., Mito, A., Takano, Y., Fujii, N., 1981. Spectral reflectance (0.25–25 μm) of powdered olivines and meteorites, and their bearing on surface materials of asteroids. In: Proc. 6th Symp. Antarct. Meteorites, Mem. Natl. Inst. Polar Res. Spec. Iss. 20, 345–361.

Miyamoto, M., Kinoshita, M., Takano, Y., 1983. Spectral reflectance (0.25–2.5 μm) of olivine and pyroxene from an ordinary chondrite. In: Proc. 8th Symp. Antarct. Meteor., Mem. Natl. Inst. Polar Res. Spec. Iss. 30, 367–377.

Moore, J.G., 1966. Rate of palagonitization of submarine basalt adjacent to Hawaii. US Geol. Surv. Prof. Paper D 550, D163–D171.

Moroz, L., Arnold, G., 1999. Influence of neutral components on relative band contrasts in reflectance spectra of intimate mixtures: Implications for remote sensing 1. Nonlinear mixing modeling. J. Geophys. Res. 104, 14109–14121.

Morris, R.V., 1989. Reflectivity spectra (350–2200 nm) of SNC meteorites. In: Proc. Lunar Planet. Sci. Conf. 20th, pp. 719–720. Abstract.

Morris, R.V., Lauer Jr., H.V., 1990. Matrix effects for reflectivity spectra of dispersed nanophase (superparamagnetic) hematite with application to martian spectral data. J. Geophys. Res. 95, 5101–5109.

Morris, R.V., Golden, D.C., 1998. Goldenrod pigments and the occurrence of hematite and possibly goethite in the Olympus–Amazonis region of Mars. Icarus 134, 1–10.

Morris, R.V., Lauer Jr., H.V., Gooding, J.L., Mendell, W.W., 1983. Spectral evidence and implications for the occurrence of aluminous iron oxides on Mars. In: Proc. Lunar Planet. Sci. Conf. 14th, pp. 526–527. Abstract.

Morris, R.V., Lauer Jr., H.V., Lawson, C.A., Gibson Jr., E.K., Nace, G.A., Stewart, C., 1985. Spectral and other physicochemical properties of submicron powders of hematite (α-Fe_2O_3), maghemite (γ-Fe_2O_3), magnetite (Fe_3O_4), goethite (α-FeOOH), and lepidocrocite (γ-FeOOH). J. Geophys. Res. 90, 3126–3144.

Morris, R.V., Lauer Jr., H.V., Agresti, D.G., Newcomb, J.A., 1986. Spectral properties of "dust" produced in the dry valleys of Antarctica. In: Dust on Mars II. LPI Publ. 86-09, 56–57. Abstract.

Morris, R.V., Agresti, D.G., Lauer Jr., H.V., Newcomb, J.A., Shelfer, T.D., Murali, A.V., 1989. Evidence for pigmentary hematite on Mars based on optical, magnetic, and Mossbauer studies of superparamagnetic (nanocrystalline) hematite 1989. J. Geophys. Res. 94, 2760–2778.

Morris, R.V., Golden, D.C., Bell III, J.F., Lauer Jr., H.V., Adams, J.B., 1993. Pigmenting agents in martian soil: inferences from spectral, Mössbauer, and magnetic properties of nanophase and other iron oxides in Hawaiian palagonitic soil PN-9. Geochim. Cosmochim. Acta 57, 4597–4609.

Morris, R.V., Golden, D.C., Bell III, J.F., 1997. Low-temperature reflectivity spectra of red hematite and the color of Mars. J. Geophys. Res. 102, 9125–9133.

Morris, R.V., Golden, D.C., Bell III, J.F., Shelfer, T.D., Scheinost, A.C., Hinman, N.W., Furness, G., Mertzman, S.A., Bishop, J.L., Ming, D.W., Allen, C.C., Britt, D.T., 2000. Mineralogy, composition, and alteration of Mars Pathfinder rocks and soils: evidence from multispectral, elemental, and magnetic data on terrestrial analogue, SNC meteorites, and Pathfinder samples. J. Geophys. Res. 105, 1757–1817.

Morris, R.V., Golden, D.C., Ming, D.W., Shelfer, T.D., Jorgensen, L.C., Bell III, J.F., Graff, T.G., Mertzman, S.A., 2001a. Phyllosilicate-poor palagonitic dust from Mauna Kea Volcano (Hawaii): a mineralogical analogue for magnetic martian dust? J. Geophys. Res. 106, 5057–5083.

Morris, R.V., Graff, T.G., Shelfer, T.D., Bell III, J.F., 2001b. Effects of palagonitic dust coatings on visible, near-IR, and Mossbauer spectra of rocks and minerals: implications for mineralogical remote sensing of Mars. In: Proc. Lunar Planet. Sci. Conf. 32nd. Abstract #1912 [CD-ROM].

Morse, S.A., 1980. Basalts and Phase Diagrams. Springer-Verlag, New York.

Mouginis-Mark, P.J., 1981. Late-stage summit activity of martian shield volcanoes. In: Proc. Lunar Planet. Sci. Conf. 12th, pp. 1431–1447.

Murchie, S., Mustard, J., Bishop, J., Head, C., Pieters, Erard, S., 1993. Spatial variations in the spectral properties of bright regions on Mars. Icarus 105, 454–468.

Mustard, J.F., Hays, J.E., 1997. Effects of hyperfine particles on reflectance spectra from 0.3 to 25 μm. Icarus 125, 145–163.

Mustard, J.F., Pieters, C.M., 1987. Quantitative abundance estimates from bidirectional reflectance measurements. In: Proc. Lunar Planet. Sci. Conf. 17th, J. Geophys. Res. 92, E617–E626.

Mustard, J.F., Pieters, C.M., 1989. Photometric phase function of common geologic minerals and applications to quantitative analysis of mineral mixture reflectance spectra. J. Geophys. Res. 94, 13619–13634.

Mustard, J.F., Sunshine, J.M., 1995. Seeing through the dust: martian crustal heterogeneity and links to the SNC meteorites. Science 267, 1623–1626.

Mustard, J.F., Erard, S., Bibring, J.-P., Head, J.W., Hurtrez, S., Langevin, Y., Pieters, C.M., Sotin, C.J., 1993a. The surface of Syrtis Major: composition of the volcanic substrate and mixing with altered dust and soil. J. Geophys. Res. 98, 3387–3400.

Mustard, J.F., Sunshine, J.M., Pieters, C.M., Hoppin, A., Pratt, S.F., 1993b. From minerals to rocks: toward modeling lithologies with remote sensing. In: Proc. Lunar Planet. Sci. Conf. 24th, pp. 1041–1042. Abstract.

Mustard, J.F., Murchie, S., Erard, S., Sunshine, J., 1997. In situ compositions of martian volcanics: implications for the mantle. J. Geophys. Res. 102, 25605–25615.

Pieters, C.M., 1983. Strength of mineral absorption features in the transmitted component of near-infrared light: first results from RELAB. J. Geophys. Res. 88, 9534–9544.

Pieters, C.M., 1989. Seeing through the dust and alteration products of Mars. In: Proc. Lunar Planet. Sci. Conf. 20th, pp. 850–851. Abstract.

Pinet, P., Chevrel, S., 1990. Spectral identification of geological units on the surface of Mars related to the presence of silicates from Earth-based near-infrared telescopic charged-couple device imaging. J. Geophys. Res. 95, 14435–14446.

Pollack, J.B., Colburn, D., Kahn, R., Hunter, J., Van Camp, W., Baldwin, B., 1977. Properties of aerosols in the martian atmosphere, as inferred from Viking Lander data. J. Geophys. Res. 82, 4479–4496.

RELAB, 1996. Reflectance Experiment Laboratory (RELAB) Description and User's Manual. Brown Univ. Press, Providence, RI.

Roush, T.L., Singer, R.B., McCord, T.B., 1987. Reflectance spectra of selected mafic silicates from 0.6 to 4.6 μm. In: Proc. Lunar Planet. Sci. Conf. 18th, pp. 854–855. Abstract.

Roush, T.L., Blaney, D.L., Singer, R.B., 1993. The surface composition of Mars as inferred from spectroscopic observations. In: Pieters, C.M., Englert, P.A.J. (Eds.), Remote Geochemical Analysis: Elemental and Mineral Composition. Cambridge Univ. Press, Cambridge, UK, pp. 367–393.

Salisbury, J.W., Hunt, G.R., Lenhoff, C.J., 1975. Visible and near-infrared spectra. X. Stony meteorites. Mod. Geol. 5, 115–126.

Schade, U., Wäsch, R., 1999. Near-infrared reflectance spectra from bulk samples of the two martian meteorites Zagami and Nakhla. Meteorit. Planet. Sci. 34, 417–424.

Sherman, D.M., Burns, R.G., Burns, V.M., 1982. Spectral characteristics of the iron oxides with application to the martian bright region mineralogy. J. Geophys. Res. 87, 10169–10180.

Singer, R.B., 1980. The dark materials on Mars. I. New information from reflectance spectroscopy on the extent and mode of oxidation. In: Proc. Lunar Planet. Sci. Conf. 11th, pp. 1045–1047. Abstract.

Singer, R.B., 1985. Spectroscopic observation of Mars. Adv. Space Res. 5, 59–68.

Singer, R.B., Roush, T.L., 1983. Spectral reflectance properties of particulate weathered coatings on rocks: laboratory modeling and applicability to Mars. In: Proc. Lunar Planet. Sci. Conf. 14th, pp. 708–709. Abstract.

Smith, J.V., Hervig, R.L., 1979. Shergotty meteorite: mineralogy, petrography and minor elements. Meteoritics 14, 121–142.

Smith, M.R., Laul, J.C., Ma, M.S., Huston, T., Verkouteren, R.M., Lipschutz, M.E., Schmitt, R.A., 1984. Petrogenesis of the SNC (shergottites, nakhlites, chassignites) meteorites: implications for their origin from a large dynamic planet, possibly Mars. In: Proc. Lunar Planet. Sci. Conf. 14th, Part 2, J. Geophys. Res. Suppl. 89, B612–B630.

Smith, P.H., Tomasko, M.G., Britt, D., Crowe, D.G., Reid, R., Keller, H.U., Thomas, N., Gliem, F., Rueffer, P., Sullivan, R., Greeley, R., Knudsen, J.M., Madsen, M.B., Gunnlaugsson, H.P., Hviid, S.F., Goetz, W., Soderblom, L.A., Gaddis, L., Kirk, R., 1997. The imager for Mars Pathfinder experiment. J. Geophys. Res. 102, 4003–4025.

Soderblom, L.A., 1992. The composition and mineralogy of the martian surface from spectroscopic observations: 0.3 to 50 μm. In: Kieffer, H.H., Jakosky, B.M., Snyder, C.W., Matthews, M.S. (Eds.), Mars. Univ. of Arizona Press, Tucson, pp. 557–593.

Solomon, S.C., Head, J.W., 1982. Evolution of the Tharsis province of Mars: the importance of heterogeneous lithospheric thickness and volcanic construction. J. Geophys. Res. 87, 9755–9774.

Stolper, E., McSween Jr., H.Y., 1979. Petrology and origin of the shergottite meteorites. Geochim. Cosmochim. Acta 43, 1475–1498.

Stolper, E., McSween Jr., H.Y., Hays, J.F., 1979. A petrogenetic model of the relationships among achondritic meteorites. Geochim. Cosmochim. Acta 43, 589–602.

Straub, D.W., Burns, R.G., Pratt, S.F., 1991. Spectral signature of oxidized pyroxenes: implications to remote sensing of terrestrial planets. J. Geophys. Res. 96, 18819–18830.

Sunshine, J.M., Pieters, C.M., 1993. Estimating modal abundances from the spectra of natural and laboratory pyroxene mixtures using the modified Gaussian method. J. Geophys. Res. 98, 9075–9087.

Sunshine, J.M., Pieters, C.M., 1998. Determining the composition of olivine from reflectance spectroscopy. J. Geophys. Res. 103, 13675–13688.

Sunshine, J.M., Pieters, C.M., Pratt, S.F., 1990. Deconvolution of mineral absorption bands: an improved approach. J. Geophys. Res. 95, 6955–6966.

Sunshine, J.M., McFadden, L.A., Pieters, C.M., 1993. Reflectance spectra of the Elephant Moraine A7001 meteorite: implications for remote sensing of planetary bodies. Icarus 105, 79–91.

Surkov, Y.A., Moskalyeva, L.P., Shcheglov, O.P., Kharyukovo, V.P., Manvelyan, O.S., Kirichenko, V.S., Dudin, A.D., 1983. Determination of the elemental composition of rocks on Venus by Venera 13 and 14 (Preliminary results). In: Proc. Lunar Planet Sci. Conf. 13th, Part 1, J. Geophys. Res. Suppl. 88, A481–A492.

Taranik, D.L., Kruse, F.A., 1989. Iron mineral reflectance in Geophysical and Environmental Research Imaging Spectrometer (GERIS) data. In: Proc. 7th Thematic Conf. Remote Sens. for Exploration Geology, pp. 445–458.

Treiman, A.H., 1990. Complex petrogenesis of the Nakhla (SNC) meteorite: evidence from petrography and mineral chemistry. In: Proc. Lunar Planet. Sci. Conf. 20th, pp. 273–280.

Wagner, J.K., Hapke, B.W., Wells, E.N., 1987. Atlas of reflectance spectra of terrestrial, lunar, and meteoritic powders and frosts from 92 to 1800 nm. Icarus 69, 14–28.

Wood, C.A., Ashwal, L.D., 1981. SNC meteorites: igneous rocks from Mars? In: Proc. Lunar Planet. Sci. Conf. 12th, pp. 1359–1375.

Wood, B.J., Banno, S., 1973. Garnet-orthopyroxene and orthopyroxene–clinopyroxene relationships in simple and complex systems. Contrib. Mineral. Petrol. 42, 109–142.

Yingst, R.A., Smith, P.H., 2000. Multispectral evidence for a single rock type at the Mars Pathfinder landing site. In: Proc. Lunar Planet. Sci. Conf. 31st. Abstract #1422 [CD-ROM].